

# 1 Evolution of the firn pack of Kaskawulsh Glacier, Yukon: meltwater 2 effects, densification, and the development of a perennial firn aquifer

3  
4 Naomi Ochwat<sup>1,5</sup>, Shawn Marshall<sup>1,2</sup>, Brian Moorman<sup>1</sup>, Alison Criscitiello,<sup>3</sup> Luke Copland<sup>4</sup>

5 <sup>1</sup>Department of Geography, University of Calgary, Calgary, Alberta, T2N 1N4, Canada

6 <sup>2</sup>Environment and Climate Change Canada, Gatineau, Quebec, K1A 0H3, Canada

7 <sup>3</sup>Department of Earth and Atmospheric Sciences, University of Alberta, Edmonton, T6G 2R3, Canada

8 <sup>4</sup>Department of Geography, Environment and Geomatics, University of Ottawa, Ottawa, Ontario K1N 6N5, Canada

9 <sup>5</sup>[Cooperative Institute for Research In Environmental Sciences, University of Colorado Boulder, Boulder, 80309, USA](#)

Naomi Ochwat 3/11/2021 7:53 PM

Formatted: Not Superscript/ Subscript

10  
11  
12 *Correspondence to:* Naomi Ochwat (naomi.ochwat@ucalgary.ca)

13  
14 **Abstract.** In spring 2018, two firn cores (21 m and 36 m in length) were extracted from the accumulation zone of  
15 Kaskawulsh Glacier, St. Elias Mountains, Yukon. The cores were analyzed for ice layer stratigraphy and density, and  
16 compared against historical measurements made in 1964 and 2006. Deep meltwater percolation and refreezing events were  
17 evident in the cores, with a total ice content of  $2.33 \pm 0.26$  m in the 36-m core and liquid water discovered below a depth of  
18 34.5 m. Together with the observed ice content, surface energy balance and firn modelling indicate that Kaskawulsh Glacier  
19 firn retained about 86% of its meltwater in the years 2005-2017. For an average surface ablation of  $0.38$  m w.e. yr<sup>-1</sup> over this  
20 period, an estimated 0.28 m w.e. yr<sup>-1</sup> refroze in the firn, 0.05 m w.e. yr<sup>-1</sup> was retained as liquid water, and 0.05 m w.e. yr<sup>-1</sup>  
21 drained or ran off. The refrozen meltwater is associated with a surface lowering of  $0.73 \pm 0.23$  m between 2005 and 2017  
22 (i.e., surface drawdown that has no associated mass loss). The firn has become denser and more ice-rich since the 1960s, and  
23 contains a perennial firn aquifer (PFA), which may have developed over the past decade. This illustrates how firn may be  
24 evolving in response to climate change in the St. Elias Mountains, provides firn density information required for geodetic  
25 mass balance calculations, and is the first documented PFA in the Yukon-Alaska region.

Shawn Marshall 3/9/2021 12:41 PM

Deleted: 73

Shawn Marshall 3/9/2021 12:38 PM

Deleted: 17

Shawn Marshall 3/9/2021 12:39 PM

Deleted: 6

Shawn Marshall 3/9/2021 12:39 PM

Deleted: 105

31 **1 Introduction**

32 With the increasing effects of climate change and the need for understanding glacier and ice sheet melt rates, geodetic  
33 methods are useful for indirect measurements of mass balance (Cogley, 2009). Based on repeat altimetry, geodetic  
34 approaches to mass balance monitoring rely on several assumptions. Estimates must be made of the density of snow, firn,  
35 and ice at the sampling location, with the additional assumption that these densities remain unchanged between the two  
36 measurement dates. However, over multi-annual timescales in a warming climate this may not be true (Moholdt et al.,  
37 2010b). Meltwater percolation and refreezing can significantly change the firn density profile and mean density of the  
38 accumulation zone of a glacier (Gascon et al., 2013), and can introduce large uncertainties when using geodetic techniques to  
39 determine glacier mass balance if they are not properly accounted for. For example, Moholdt et al. (2010a) determined the  
40 geodetic mass balance of Svalbard glaciers to be  $-4.3 \pm 1.4 \text{ Gt yr}^{-1}$ , based on ICESat laser altimetry, with the large  
41 uncertainty attributed to limited knowledge of the snow and firn density and their spatial and temporal variability. By  
42 altering the density and causing surface lowering, meltwater percolation, refreezing, and liquid water storage all complicate  
43 the interpretation of geodetic mass balance data.

44  
45 Warming firn can result in increased meltwater production and altered firn densification processes. Initially, melt can round  
46 the snow grains and increase the snowpack density, and then percolate into the firn and refreeze as ice layers or lenses  
47 (Sommerfeld and LaChapelle, 1970; Cuffey and Paterson, 2010). On glaciers with medium to high surface melt, and high  
48 annual snow accumulation, meltwater that percolates below the winter cold layer often will not refreeze, and may thus form  
49 a perennial firn aquifer (PFA) if this water cannot effectively drain through crevasses or moulins (Kuipers Munneke et al.,  
50 2014). These internal accumulation processes can significantly increase the firn density, and once ice layers or PFAs form  
51 they affect how meltwater percolates through the firn pack (Gascon et al., 2013). Due to the spatial heterogeneity of  
52 meltwater retention, percolation, and refreezing processes, there are still many gaps in knowledge of how to model these  
53 processes and subsequently estimate firn density in areas where these processes occur (van As et al., 2016).

54  
55 Meltwater retention in firn is also important for estimating glacial runoff contributions to sea level rise. Numerous recent  
56 studies have investigated meltwater refreezing processes in northern locations such as southern Greenland (Humphrey et al.,  
57 2012; Harper et al., 2012; De La Peña et al., 2015; MacFerrin et al., 2019; Vandecrux et al., 2020), Canadian Arctic  
58 Archipelago (Noël et al. 2018, Zdanowicz et al., 2012; Bezeau et al., 2013; Gascon et al., 2013), and Svalbard (Noël et al.  
59 2020, Van Pelt et al., 2019, Christianson et al., 2015). In many locations with cold deep firn, short term increases in surface  
60 melt rates may not result in proportional increases in surface runoff due to percolation and refreezing of meltwater in the firn  
61 pack (e.g., Harper et al., 2012; Koenig et al., 2014; MacFerrin et al., 2019). However, in the long term this may lead to  
62 expansion of low-permeability ice layers, causing run-off to increase and expediting the movement of water from glaciers to  
63 the ocean (MacFerrin et al., 2019, Machguth et al., 2016). Current knowledge of these processes is limited for mountain

Luke Copland 3/8/2021 10:44 AM  
Deleted: (Cuffey and Paterson, 2010). Meltwater  
can

Naomi Ochwat 3/6/2021 5:27 PM  
Deleted: ,

67 glaciers in other regions, although this information is required for improved estimates and models of glacier mass balance  
68 and associated sea-level rise.  
69  
70 In this study two firm cores were retrieved in spring 2018 on Kaskawulsh Glacier, St. Elias Mountains, Yukon, and analyzed  
71 for density and the effects of meltwater percolation and refreezing. [We also use a firm model \(Samimi et al., 2020\) forced by](#)  
72 [bias-adjusted ERA climate reanalyses to investigate the evolution of the firm through time at this location.](#) Comparisons of  
73 these measurements with firm density profiles collected at a nearby site in 1964 and 2006 enable us to: (i) quantify  
74 contemporary firm characteristics and densification processes; (ii) determine how the physical properties of the firm pack  
75 have changed over the past ~50 years; and (iii) assess the potential widespread presence of a PFA on the upper Kaskawulsh  
76 Glacier.

## 77 2 Study area

78 The St. Elias Mountains are located in the southwest corner of Yukon Territory, Canada, and contain many peaks higher than  
79 3000 m, including the highest mountain in Canada, Mount Logan, at 5959 m a.s.l. (Figure 1). The St. Elias is home to the  
80 largest icefield outside of the polar regions, with an area of ~46,000 km<sup>2</sup> (Berthier et al., 2010). Measurements presented  
81 here are focused on the upper accumulation zone of Kaskawulsh Glacier (Figure 1), which is part of an extensive (~63 km<sup>2</sup>)  
82 snowfield at an elevation of 2500-2700 m a.s.l. This plateau region has subtle topographic variations and includes the  
83 drainage divide between the Kaskawulsh and Hubbard Glaciers.

84  
85 Kaskawulsh Glacier is a large valley glacier located on the eastern side of the St. Elias Mountains within the Donjek Range,  
86 and is approximately 70 km long and 3-4 km wide. Our 2018 drill site was located on the upper north arm of the glacier in  
87 the accumulation zone (60.78°N, 139.63°W), at an elevation of 2640 m a.s.l. Based on satellite imagery, Foy et al. (2011)  
88 estimated an average equilibrium line altitude (ELA) for the glacier of 1958 m a.s.l. for the period 1977-2007, while Young  
89 et al. (2020) provided a mean ELA of 2261 ±151 m a.s.l. for the years 2013-2019. Our core site is thus well above the ELA,  
90 and has remained within the main accumulation area of the glacier. Mean annual and summer (JJA) air temperatures from  
91 1979-2019 were -10.7°C and -2.5°C, respectively, based on bias-adjusted ERA5 climate reanalyses (Hersbach et al., 2020).  
92 The main melt season occurs from June through August. Over the period 1979-2016, Williamson et al. (2020) reported that  
93 the St. Elias Icefield air temperature warmed at an average rate of 0.19°C decade<sup>-1</sup> at an elevation of 2000-2500 m a.s.l.,  
94 rising to 0.28°C decade<sup>-1</sup> at an elevation of 5500-6000 m a.s.l.

95  
96 Previous studies of Kaskawulsh Glacier have included an analysis of volume change over time based on comparisons of  
97 satellite imagery and digital elevation models (Foy et al., 2011; Young et al., 2020). Several reports in the 1960s documented  
98 various glaciological characteristics and processes occurring in the St. Elias Icefields, as part of the Icefield Ranges Research

Shawn Marshall 3/9/2021 1:02 PM

Deleted: d

Shawn Marshall 3/9/2021 1:03 PM

Deleted: general

Shawn Marshall 3/9/2021 1:03 PM

Deleted: ERA

Naomi Ochwat 3/6/2021 5:29 PM

Deleted: and temperatures

Shawn Marshall 3/9/2021 1:06 PM

Deleted: Q

Shawn Marshall 3/9/2021 1:06 PM

Deleted: D

Shawn Marshall 3/9/2021 1:06 PM

Deleted: A

Shawn Marshall 3/9/2021 1:07 PM

Deleted: likelihood of a

107 Project (IRRP) (Wood, 1963; Grew and Mellor, 1966; Marcus and Ragle, 1970). Firn density and temperature measurements  
108 to 15-m depth were made during this period at site IRRP A, near the Kaskawulsh-Hubbard divide and about 5 km from our  
109 core site. Additional snow accumulation data are available from the ‘Copland Camp’ site on the upper Hubbard Glacier,  
110 located ~12 km southwest of our drill site and at a similar elevation (Figure 1). A weather station located on a nunatak near  
111 to Copland Camp has been in service since 2013 (60.70°N, 139.80°W, ~2600 m a.s.l.; Figure 1). Other relevant studies in the  
112 region include ice cores collected from the Eclipse Icefield, located 12 km northwest of our drill site (Yalcin et al., 2006;  
113 Zdanowicz et al., 2014) but at a higher elevation (3017 m a.s.l.).

114  
115 We consider snow accumulation rates, weather conditions, and earlier firn core studies across several different locations  
116 within this broad snowfield region that constitutes the upper accumulation areas of the Kaskawulsh and Hubbard Glaciers.  
117 Some caution is needed in comparing different sites, but the region is relatively flat and uniform, with the exception of some  
118 nunataks. Away from the nunataks there is negligible influence from topographic obstacles or valley walls, so we  
119 hypothesize that the upper accumulation area will be exposed to similar climate conditions and snow accumulation rates over  
120 long periods. The possibility of significant spatial variability cannot be ruled out, however, so we consider this further in the  
121 data analysis.

122

### 123 3 Methods

#### 124 3.1 Ice core field collection

125 Two 8-cm diameter cores were drilled between May 20<sup>th</sup> and 24<sup>th</sup>, 2018, using an ECLIPSE ice drill (Icefield Instruments,  
126 Whitehorse, Yukon). With a starting depth of 2 m below the snow surface, Core 1 was 34.6 m long and reached a depth of  
127 36.6 m, and Core 2 was 19.6 m long and reached a depth of 21.6 m. The two cores were drilled 60 cm apart, and core  
128 stratigraphy and density were recorded in the field. At a depth of 34.5 m below the snow surface, liquid water became  
129 evident in Core 1; drilling was stopped at a depth of 36.6 m to avoid the risk of the drill freezing in the hole.

130  
131 Once the cores were retrieved the presence of ice layers, ice lenses and “melt-affected” firn was logged and the stratigraphic  
132 character (e.g., texture, opacity), depth, and thickness were recorded. Melt-affected firn refers to any firn that displays  
133 physical characteristics indicating that there was the presence of liquid water at some point (Figure S5). This can result in ice  
134 layers, ice lenses, or can be indicated by the lack of grain boundaries, the presence of air bubbles, and opacity. When an ice  
135 horizon extended across the entire diameter of the core, it was labeled as an ice layer. If the ice horizon was of more limited  
136 lateral extent, it was labeled an ice lens. Ice lenses were occasionally wedge shaped.

137  
138 All of the density measurements for Core 1 were completed in the field. The Core 2 samples could not be measured for

Luke Copland 3/8/2021 10:51 AM  
Deleted: -



140 density in the field due to lack of time, and were flown to Kluane Lake Research Station frozen, where the measurements  
 141 were made within 24 hours of arrival. A random assortment of 125 out of the 196 Core 2 sample bags were damaged during  
 142 this transport, and were not included in the measurements. This left a random reduced set of samples available to use for the  
 143 density analysis, so we were able to construct a density stratigraphy (Core 2 in Figure 2B), but uncertainties are higher for  
 144 Core 2 and most of our analysis therefore focuses on Core 1.

### 146 3.2 Ice core density analysis

147 Ice core density measurements were completed in the field. Each core was sawed into ~10-cm long sections, and the diameter  
 148 of the sections measured at each end. The sections were then double bagged, weighed, and assessed for the quality of the  
 149 core sample and its cylindrical completeness, which we denote  $f$ . The average diameter was used to determine the volume of  
 150 the core section ( $V$ ). Together with the mass of the core section,  $m$ , density was calculated following:

$$152 \quad \rho = m/V, \text{ with } V = f\pi L(D/2)^2, \quad (1)$$

153 where  $\rho$  is the density of the firm,  $D$  is the average core section diameter,  $L$  is the length of the section, and  $f \in [0,1]$  is the  
 154 subjectively assessed fraction of completeness of the core section. For example, if visual inspection indicated that about 5%  
 155 of the core was missing (e.g., due to missing ice chips caused by the core dogs of the drill head), then  $f$  would be 0.95.  
 156 Outliers were removed for the background firm density calculations if they were not physically possible (i.e., values  $>917 \text{ kg}$   
 157  $\text{m}^{-3}$  or  $<300 \text{ kg m}^{-3}$  at depths below the last summer surface). Outliers from 32-36 m depth had residual liquid water in them,  
 158 so these higher density values were retained.

160  
 161 In order to calculate the uncertainty in density,  $d\rho$ , random and systematic sources of error have to be taken into account in  
 162 the propagation of errors:

$$163 \quad d\rho = \rho \sqrt{\left(\frac{dm}{m}\right)^2 + \left(\frac{dV}{V}\right)^2} . \quad (2)$$

164 The mass uncertainty was assumed to be 0.3 g, which is a conservative estimate given the scale's accuracy ( $\pm 0.1 \text{ g}$ ), but  
 165 accounts for potential residual snow or water on the scale. The volume uncertainty is calculated by breaking down Eq. (1) for  
 166 sample volume,  $V = fAL$ , where cross-sectional area  $A = \pi(D/2)^2$ . There is uncertainty in the measured length of the core  
 167 section,  $L$ , the radius of the core section,  $D/2$ , and the assessment of the completeness of the core sample,  $f$ . Each of these  
 168 was calculated independently and the propagation of uncertainty was calculated from:

$$170 \quad dV = V \sqrt{\left(\frac{df}{f}\right)^2 + \left(\frac{dA}{A}\right)^2 + \left(\frac{dL}{L}\right)^2} . \quad (3)$$

Naomi Ochwat 3/6/2021 5:37 PM  
 Deleted: ,

Naomi Ochwat 3/6/2021 5:34 PM  
 Deleted: so

Naomi Ochwat 3/6/2021 5:37 PM  
 Deleted: ,

Naomi Ochwat 3/6/2021 5:37 PM  
 Deleted: so

Shawn Marshall 3/9/2021 1:12 PM  
 Deleted: 71

Shawn Marshall 3/9/2021 1:13 PM  
 Deleted: with at least one sample available per meter except

Naomi Ochwat 3/6/2021 5:36 PM  
 Deleted: for between 13.29 and 14.95 m

Shawn Marshall 3/9/2021 1:14 PM  
 Deleted: Due to these missing values, only bulk density values are presented for Core 2.

Luke Copland 3/8/2021 10:54 AM  
 Deleted: in the field,

182  $dL$  was assumed to be 0.25 cm because the tape measure had ticks at every mm so it could be measured with precision, but  
 183 core sections were often uneven, with crumbly edges caused by the drill cutters. The same uncertainty was assigned to the  
 184 measurement of core diameter. Given two independent measurements, the uncertainty in the diameter is  $dD =$   
 185  $\frac{1}{2}\sqrt{(0.25)^2 + (0.25)^2} = 0.18$  cm. For the cross-sectional area, the uncertainty  $dA = \pi DdD/2$ .  
 186  
 187 Values of  $f$  were determined by assessing the shape of the core and deciding how complete a cylinder the core section  
 188 represented (e.g., accounting for missing volume due to chips from the core dogs along the edges). Three different people  
 189 performed this evaluation, so there was subjectivity in each of the  $f$  values and it is best to be conservative with this estimate.  
 190 We assigned this to be  $df = 0.2$  for  $f < 0.8$  and  $df = 0.1$  for  $f \geq 0.8$ . The uncertainty of a higher  $f$  value is lower, because when  
 191 a core was of good quality it was obvious. Less complete cylinders were more difficult to assess, hence the greater  
 192 uncertainty when  $f \leq 0.8$ . The  $f$  value has the greatest effect on the overall uncertainty calculation for firm density. We did not  
 193 record  $f$  values for Core 2 in the field, so values are based on the measurements from Core 1. The minimum value recorded  
 194 in Core 1 was  $f = 0.7$ , with a maximum of 1 and an average of 0.96. We assume a value of  $f = 0.96 \pm 0.1$  for all of Core 2.  
 195  
 196 The resulting uncertainty in the density was calculated from:

$$d\rho = \rho \sqrt{\left(\frac{dm}{m}\right)^2 + \left(\frac{dv}{v}\right)^2} . \quad (4)$$

197  
 198 For the average densities,  $\bar{\rho}$ , the uncertainty can be calculated from the standard error of the mean,  $d\bar{\rho} = d\rho/\sqrt{N}$ , for sample  
 199 size  $N$ . This can be estimated from the average value of  $d\rho$ , but we report the more precise uncertainty calculated from the  
 200 root-mean square value of all point values,  $d\bar{\rho} = \frac{1}{N}[\sum_N d\rho_k^2]^{1/2}$ . Density can be expressed as water equivalence (w.e.)  
 201 for each core section from the conversion  $w = L\rho/\rho_w$ , where  $\rho_w$  is the density of water. For the whole core, of length  $L_c$ , the  
 202 water equivalence is  $w_c = L_c\bar{\rho}/\rho_w$ , with units m w.e. We also include an estimate of the age of the cores, based on an  
 203 estimate of the average annual net accumulation rate,  $\bar{a}$ , with units m w.e.  $\text{yr}^{-1}$ . The age of the core is then  $\tau_c = w_c/\bar{a}$ .  
 204 Uncertainty is estimated by propagation of uncertainties in  $w_c$  and  $\bar{a}$ . We use an uncertainty of  $dL_c = 0.5$  m for the total  
 205 length of the core,  $L_c$ , which is based on measurements during retrieval of Core 1 of 35.05 m from the drill panel, 34.59 m  
 206 from the addition of core lengths, and 34.25 m from the sum of the  $\sim 10$  cm samples. For Core 2 the length was 19.75 m from  
 207 the drill panel, 19.35 m from the addition of core lengths, and 19.63 m from the sum of the  $\sim 10$  cm samples.

208  
 209 Ice fraction,  $F_i \in [0,1]$ , was calculated for each 10-cm section of the firm core. Here ice was defined based on its lack of air  
 210 bubbles and crystalline structure, as compared to the granular structure of firm. We refer to this as ice fraction, rather than  
 211 melt percent, as melt percent generally assumes that the meltwater remains within the net annual accumulation layer

212 (Koerner, 1977), which cannot be assumed here due to evidence that meltwater percolates beyond the annual accumulation  
213 layer and refreezes into previous years' accumulation. The thickness of individual ice layers was summed within each 10-cm  
214 core section. In core samples that had ice lenses, their diameter typically occupied about 50% of the core sample; therefore  
215 their thickness was divided by two before being summed. For each core section, total ice content was divided by the length  
216 of the section,  $L$ , to give  $F_i$ . These values were also summed to give the total ice core ice content.

217  
218 To understand the firn densification process in the absence of refrozen meltwater, the 'background' firn density is of interest.  
219 For each sample, we estimated this by subtracting the mass and volume of the ice to give the firn density in the absence of  
220 ice content. We used a 30-cm moving average of total ice content and density in order to smooth out a possible error of  $\pm 10$   
221 cm in assigning the location of the ice features within the stratigraphy. Each sample had a measured bulk density,  $\rho_b$ , which  
222 we assume resulted from a binary mixture of ice and firn, with densities  $\rho_f$  and  $\rho_i$ . Ice and firn fractions,  $F_i$  and  $F_f$ , were  
223 defined with  $F_i + F_f = 1$ . The background firn density was then calculated following:

224 
$$\rho_f = (\rho_b - \rho_i F_i) / F_f. \quad (5)$$

225 In cases where there was no ice fraction ( $F_i = 0$ ),  $\rho_f = \rho_b$ . Ice layers and lenses were assumed to have a density of  $874 \pm 35$   
226  $\text{kg m}^{-3}$ , based on the average density of firn-core sections that were 100% ice in Greenland ( $873 \text{ kg m}^{-3}$ ) and Devon Ice Cap  
227 ( $875 \text{ kg m}^{-3}$ ) (Bezeau et al., 2013; Machguth et al., 2016). This is different from the  $917 \text{ kg m}^{-3}$  upper bound used in the  
228 outlier analysis because that is the theoretical limit for pure ice, whereas  $874 \text{ kg m}^{-3}$  is based on measured field data which  
229 includes observed ice layers and lenses which have small bubbles and imperfections in them.

230  
231 There is surface lowering associated with melting but without associated mass loss, due to subsurface refreezing. This  
232 surface lowering is an 'apparent ablation' in airborne or satellite altimetry signals. We calculated this for each core section  
233 using the background firn density,  $\rho_f$ , and length of the section,  $L$ . The 'thinning' or surface lowering of a given core  
234 section,  $\Delta L$ , was estimated by reverting the ice to the density of the background firn, following:

235  
236 
$$\Delta L = L \left[ \left( F_f + \frac{\rho_i F_i}{\rho_f} \right) - 1 \right]. \quad (6)$$

237 Summed over the full firn column, this gives the total surface lowering associated with meltwater that percolates and  
238 refreezes, with no actual loss of mass.

239  
240  
241

242 **3.3 Historical measurements**

243 As part of an expedition undertaken by the IRRP, Grew and Mellor (1966) measured snow density and temperature to a  
244 depth of 15 m at the Divide site on July 23, 1964 (Fig. 1). The first ~4 m were measured in a snow pit, while the remaining  
245 ~11 m were based on measurements of a core drilled with a Cold Regions Research and Engineering Laboratory (CRREL)  
246 coring auger. The original data is not available, so values were reconstructed based on digitization of the density plot  
247 provided in Figure 4 of Grew and Mellor (1966). This digitization was undertaken with WebPlot Digitizer 4.3 (Rohatgi,  
248 2020), and has an estimated error of  $\pm 2 \text{ kg m}^{-3}$  for density and  $\pm 0.01 \text{ m}$  for depth. Errors were calculated by clicking the  
249 same point 25 times and evaluating the variability of the points (i.e., the standard deviation).

250  
251 From July 14-17, 2006, snow density and temperature measurements were recorded every 10 cm to a depth of 10.4 m at the  
252 Copland Camp as part of a University of Ottawa field class. Measurements from 0 to 5.4 m were recorded in a snow pit,  
253 while those from 5.5 to 10.4 m were based on a core recovered with a Kovacs Mark II coring system (Kovacs Enterprises,  
254 Oregon, USA). Density measurements in the snow pit were undertaken with a  $250 \text{ cm}^3$  RIP 2 Cutter (Snowmetrics,  
255 Colorado, USA), and in the ice core by measuring and weighing core sections and using Eq. (1). Errors in the density  
256 measurements were determined from Eq. (4), and verified against density values recorded in a second snow pit dug to a  
257 depth of 4.0 m, approximately 2 m away from the first. All temperature measurements were undertaken with a Thermor  
258 PS100 digital stem thermometer with an accuracy of  $\pm 0.5^\circ\text{C}$ .

259  
260 Annual snow accumulation at the Copland Camp was measured between 2004-2011 with a Campbell Scientific SR50 Sonic  
261 Ranging Sensor mounted on a cross-arm on a vertical steel pole drilled into the firn. The SR50 was connected to a Campbell  
262 Scientific CR10X logger, and included a correction for the change in speed of sound with air temperature. The mounting  
263 pole was raised annually to keep it above the snow surface, and densities recorded in snow pits collected during annual  
264 University of Ottawa field classes (typically in early July) were used to convert the SR50 depth measurements into w.e.  
265 values.

266  
267 **3.4 Energy balance and firn modelling**  
268 ERA climate reanalyses were used to examine changes in climate and annual surface melting at the study site since the  
269 1960s, coupled with a firn model to simulate the decadal evolution of firn temperature, hydrology, ice content, and density.  
270 Daily melt rates were calculated from 1965 to 2019 using a surface energy balance model (Ebrahimi and Marshall, 2016),  
271 coupled to a subsurface model of coupled thermal and hydrological evolution in the snow and firn (Samimi et al., 2020). The  
272 model calculates the surface energy budget and snow melt based on incoming shortwave and longwave radiation,  
273 temperature, relative humidity, wind speed, and air pressure, with internal parameterizations of surface albedo evolution and  
274 outgoing longwave radiation. Conductive heat flux to the snow surface and snow surface temperatures are simulated within  
275 the subsurface snow/firn model. Snow and firn densification are parameterized following Vionnet et al. (2012) for the firn

276 matrix ('background firm'), with bulk density including the additional mass of any ice or water content. Details of the model  
277 are provided in the Supplementary Information.

278  
279 Meteorological inputs for the surface energy balance model were derived from the ERA5 climate reanalysis for the period  
280 1979 to 2019 (Hersbach et al., 2020), and extended back to 1965 using the ERA 20<sup>th</sup> century reanalysis (ERA20c; Poli et al.,  
281 2016). ERA5 outputs are at a resolution of 0.25° latitude and longitude, and data for our analysis was averaged from ERA5  
282 grid cells located at (60.75°N, 139.75°W) and (60.75°N, 139.5°W). ERA20c data are at 1° latitude and longitude resolution,  
283 and we interpolated meteorological conditions to the upper Kaskawulsh Glacier from the four model grid cells at 60° to  
284 61°N and 139° to 140°W. ERA20c fields were homogenized with ERA5 through bias adjustments for two years of overlap  
285 in the reanalyses, 1979 and 1980, with ERA5 assumed to be the more accurate reconstruction. Monthly bias adjustments  
286 based on this period of overlap were then applied to the ERA20c data from 1965 to 1978.

287  
288 The reanalysis data represent the climatology over the region of the upper Kaskawulsh-Hubbard divide (i.e., a 0.25° grid  
289 cell), and are not specific to our core site. The firm modelling is therefore taken to be generally applicable for this upper  
290 plateau region. ~~ERA air pressure and 2-m temperature, and humidity, fields were~~ bias-adjusted to the specific elevation of our  
291 core site, 2640 m (see the Supplementary Information). ERA5 temperature fields were evaluated against Copland weather  
292 station data from 2014-2018, which indicate a small (0.6°C) cold bias in the ERA5 data for average summer (JJA)  
293 temperatures over this period. ERA temperatures were further bias-adjusted by this amount. Our firm core site, the Copland  
294 weather station, Copland Camp, and IRRP research sites all fall within the same ERA5 grid cell, and we make the  
295 assumption that climate conditions are similar for similar elevations and glaciological settings within this region.

296  
297 Surface energy balance and melt were calculated every 30 minutes, using mean daily meteorological forcing from ERA and  
298 a parameterization of the diurnal cycles of temperature and incoming shortwave radiation (Ebrahimi and Marshall, 2016).  
299 ~~Snow accumulation is based on the ERA total precipitation, with a constant scaling factor of 1.6 in order to give~~  
300 ~~representative annual totals. With this scaling, mean annual precipitation at the site ( $\pm 1$  standard deviation) was  $1.83 \pm 0.32$~~   
301 ~~m w.e. yr<sup>-1</sup>. Snow is updated monthly in the numerical simulation. We neglect rainfall, as we don't have a good constraint on~~  
302 ~~how much summer precipitation falls as rain and this will not be reliably predicted in the climate reanalysis. Summer~~  
303 ~~temperatures are cool (mean value of  $-2.4^{\circ}\text{C}$ ) and during our experience working at the Copland Camp in the month of July,~~  
304 ~~we have experienced numerous snow events but no rainfall. While rain must occur from time to time, we believe it to be rare~~  
305 ~~at the study site.~~

306  
307 Subsurface temperatures were modelled for a 35-m firm column, with a simple model for meltwater percolation that accounts  
308 for meltwater refreezing and the associated latent heat release where snow or firm is below 0°C (Samimi and Marshall, 2017;

Shawn Marshall 3/9/2021 1:28 PM  
**Deleted:** However,  
Shawn Marshall 3/9/2021 1:28 PM  
**Deleted:** meteorological conditions (  
Shawn Marshall 3/10/2021 11:39 AM  
**Deleted:** , pressure,  
Shawn Marshall 3/9/2021 1:28 PM  
**Deleted:** )  
Shawn Marshall 3/9/2021 1:28 PM  
**Deleted:** are

Shawn Marshall 3/9/2021 4:11 PM  
**Formatted:** Superscript  
Shawn Marshall 3/9/2021 4:11 PM  
**Formatted:** Superscript

Shawn Marshall 3/9/2021 4:07 PM  
**Deleted:**  
Luke Copland 3/8/2021 11:04 AM  
**Deleted:** -

316 Samimi et al., 2020). For the current study, we discretize the snow and firn into 58 layers from 0.1 to 1 m in thickness, with  
317 higher resolution near the surface. The firn model is coupled with the surface energy balance model, solving for the firn  
318 thermodynamic and hydrological evolution at 30-minute time steps for the period 1965 to 2019. The subsurface temperature  
319 evolution includes vertical heat conduction and latent heat release from refreezing. Heat advection associated with snow  
320 accumulation is neglected. When subsurface temperatures reach 0°C, liquid water is retained or percolates to depth,  
321 following a Darcian parameterization for water flux:  $q_w = -k_h \nabla \phi$ , for hydraulic conductivity  $k_h$  and hydraulic potential  $\phi$   
322 (Samimi and Marshall, 2017). For the numerical experiments in this study we set  $k_h = 10^5 \text{ m s}^{-1}$  in snow and  $10^6 \text{ m s}^{-1}$  for  
323 snow and firn, respectively. Capillary water retention is calculated following Coléou and Lesaffre (1998). The default model  
324 parameters are based on calibration at DYE-2, Greenland, in the percolation zone of the southern Greenland Ice Sheet  
325 (Samimi et al., 2020). A broader range of model parameters is explored in sensitivity analyses presented in the  
326 Supplementary Information.

327  
328 The model is ‘spun up’ through a 30-year simulation with perpetual 1965 climate forcing (i.e., running through 30 annual  
329 cycles with 1965 climate conditions). This provides the initial temperature, density, and ice-layer structure within the firn  
330 column. Ideally, a spin-up simulation forced by the historical meteorological conditions (e.g., the years 1935-1965) would be  
331 preferable to assuming a perpetual climatology from a single year. Mean annual and mean summer temperatures were  
332 normal in 1965, so the model results are not strongly sensitive to this assumption (discussed in the results), but we explore a  
333 range of numerical experiments to examine the model sensitivity to these initial conditions and the spin-up assumptions.

334

## 335 4 Results

### 336 4.1 Ice core density

337 The density data are plotted in Figure 2, fitted with a logarithmic curve to quantitatively compare our two cores. The first 4.2  
338 m of both 2018 cores was dry and had an average density of  $450 \pm 21 \text{ kg m}^{-3}$ , with no ice content. At 4.2 m there was a  
339 significant ice crust, with large crystal size, rounded grains and high impurity content, which was assumed to represent the  
340 last summer surface (LSS) from 2017. The snow above this LSS layer was therefore classified as seasonal snow. In this  
341 section we focus on the firn characteristics below the LSS, so our discussion is centered on the core recovered between 4.2  
342 and 36.6 m below the surface for Core 1 (i.e., total firn length of 32.4 m), and between 4.2 and 21.6 m below the surface for  
343 Core 2 (i.e., total firn length of 17.4 m). For consistency, we reference all depths to the seasonal snow surface throughout  
344 this paper.

345  
346 In the upper 10 m of firn (4.2 to 14.2 m below the surface; Table 1), Cores 1 and 2 had average densities of  $588 \pm 8 \text{ kg m}^{-3}$   
347 and  $572 \pm 7 \text{ kg m}^{-3}$ , respectively, giving an overall average density of  $580 \pm 5 \text{ kg m}^{-3}$ . Over the upper 17.4 m of firn in each

Shawn Marshall 3/9/2021 4:34 PM

Deleted: Sensitivity tests

Shawn Marshall 3/9/2021 4:34 PM

Deleted: within the Supplementary Information als

350 core (4.2 m to 21.6 m below the surface; the depth to the bottom of Core 2), Kaskawulsh firn had an average density of 632  
351  $\pm 4 \text{ kg m}^{-3}$ . The full 32.4 m of firn at Core 1 (4.2 to 36.6 m below the surface) had an average density of  $698 \pm 5 \text{ kg m}^{-3}$ . Ice  
352 content generally increased with depth in the upper  $\sim 25$  m of the core, but deeper sections were less icy (Table 1). The  
353 bottom 5 m of firn in Core 1 had an average density of  $826 \pm 13 \text{ kg m}^{-3}$ , but with no identified ice layers. Based on the high  
354 density and texture of this deep firn, along with the presence of liquid water in the deepest sections of the core, we believe  
355 that we drilled to near the base of the firn at the core site, but cannot confirm this as we halted drilling before reaching  
356 glacier ice.

357  
358 Total ice content in the 32.2 m firn portion of Core 1 (4.2 to 36.6 m below the surface) was  $2.33 \pm 0.26 \text{ m}$  of ice or  $2.67 \pm$   
359  $0.24 \text{ m w.e.}$  This is equivalent to 7.2% by volume and 11.9% by mass (Table 1). Using Eq. (5) and the values for ice content  
360 in Core 1, we estimate a background firn density of  $676 \pm 6 \text{ kg m}^{-3}$  for the full column of firn, 3.2% less than the bulk density  
361 of the firn (Table 1). The two cores had very similar bulk and background densities over the upper 10 m of firn (4.2 to 14.2  
362 m below the surface) and 17.4 m (4.2 to 21.6 m below the surface), where a direct comparison was possible. The total water  
363 equivalent of firn in Core 1 was calculated to be  $w_e = 22.5 \pm 0.2 \text{ m w.e.}$

364

#### 365 4.2 Ice core stratigraphy

366 The stratigraphy of the 2018 cores indicates numerous ice layers as well as melt-affected firn, distinguished by a lack of  
367 grain boundaries or opaque, bubbly firn. The first 4.2 m comprised the seasonal snowpack, with firn below. Within the first 6  
368 m below the surface there were several small ice layers ( $< 2.5 \text{ cm}$  thick), interpreted as wind crusts (Figure 3). Several thick  
369 ( $> 10 \text{ cm}$ ) ice layers were found between 6 and 26 m depth (1.8 to 21.8 m in the firn). The largest ice layer in Core 1 was 22  
370 cm thick, found at 14.1 m (9.9 m in the firn). At 26.4 m (22.2 m in the firn) the ice layers and lenses disappeared. Below this  
371 the firn was almost entirely meltwater-affected, based on its appearance and texture, but without the quantity of ice lenses or  
372 ice layers that were present in the first 25 m. We interpret this section of the core as infiltration ice, consisting of water-  
373 saturated firn that has experienced refreezing. At 30 m depth (25.8 m in the firn), the meltwater effects were absent and there  
374 were two small ice layers and an ice lens. At 30.6 m depth the firn was melt-affected again. From 34.5 to 36.6 m (30.3 to  
375 32.4 m in firn) the core sections expelled liquid water as they were extracted from the core barrel.

376

377 In Core 2 there were numerous ice layers starting at a depth of 3.8 m, and below 4.4 m (0.2 m in the firn) the core was  
378 meltwater-affected. There was a thick ice layer at 6.6 m (2.4 m in the firn) that was 30 cm lower than a similar ice layer in  
379 Core 1 at 6.3 m. There were numerous melt-affected layers between ice lenses much closer to the surface in Core 2 than  
380 Core 1. In Core 1 there were several ice layers at  $\sim 10$  m depth (5.8 m in the firn), but these layers were not present in Core 2.  
381 At 14.4 m (10.2 m in the firn) another section of the firn had numerous ice layers ( $\sim 20$ -30 cm deeper than recorded in Core  
382 1), and at 14.6 m the thickest ice layer was encountered (12 cm), corresponding well with the thickest layer in Core 1.

383 Between 16 and 21.5 m (11.8 to 17.3 m in the firn) the core was melt-affected. We attribute differences between Core 1 and  
384 Core 2 stratigraphy to uncertainty in the depth of features (as discussed in Section 3.2), and horizontal variability in  
385 meltwater infiltration, which is known to occur at length scales less than 1 m (Parry et al., 2007; Harper et al., 2011). [Spatial  
386 heterogeneity in firn is common in areas with high surface melt due to differential melting and percolation that is complex  
387 due to the presence of sastrugi and wind crusts, different permeability of the snow and firn, and vertical piping mechanisms  
388 \(Marchenko et al., 2017; Parry et al., 2007\).](#)

Luke Copland 3/8/2021 11:19 AM

Deleted: amounts of

### 390 4.3 Changes in firn characteristics over time

391 The firn in the accumulation area of Kaskawulsh Glacier has become denser since 1964 (Figure 4a). The mean density of the  
392 upper 7 m of firn was  $516 \text{ kg m}^{-3}$  in 1964 (3.3 to 10.3 m below the surface),  $590 \text{ kg m}^{-3}$  in 2006 (3.5 to 10.5 m below the  
393 surface) and  $549 \text{ kg m}^{-3}$  in 2018 (4.4 to 11.4 m below the surface). The difference between the average densities from the  
394 upper 7 m of the 1964 and 2018 core is  $33 \text{ kg m}^{-3}$ , which is an increase of  $\sim 7\%$ . It is difficult to assess whether firn  
395 temperatures have changed over this time, as limited data are available from below the depth of the annual temperature wave  
396 ( $\sim 10$  m for heat diffusion, and deeper than this with the effects of subsurface meltwater infiltration and latent heat release).  
397 Borehole temperature records from Grew and Mellor (1966) indicate temperate ( $0^\circ\text{C}$ ) conditions at 15-m depth in the  
398 summer of 1964, which suggests that deep temperate firn may have existed at this site in the 1960s. This supports the  
399 assumption that Kaskawulsh Glacier is temperate (Foy et al., 2011), despite mean annual air temperatures of about  $-11^\circ\text{C}$  on  
400 the upper glacier.

Luke Copland 3/8/2021 11:21 AM

Deleted: in

401  
402 Accumulation data from the IRRP A site, Copland Camp and our 2018 measurements do not show any evidence for a  
403 significant change over time, although there can be high interannual variability. At IRRP A, Wagner (1969) reported values  
404 between 1.3 m to 1.9 m w.e.  $\text{yr}^{-1}$  for 1963. Marcus and Ragle (1970) measured a winter snow accumulation of 1.6 m w.e.  
405 from 1964-1965. Holdsworth (1965) reported an estimated mean annual accumulation rate of 1.8 m w.e.  $\text{yr}^{-1}$  in the early  
406 1960s (year not specified) (Holdsworth, 1965). Yearly snow accumulation data from 2004-2011 collected with the SR50 at  
407 Copland Camp indicate a mean annual accumulation rate of 1.77 m w.e.  $\text{yr}^{-1}$ , with variations between 1.3 and 2.4 m w.e.  $\text{yr}^{-1}$ .  
408 The seasonal snowpack at our drill site was 4.2 m in May 2018, with an average snow density of  $440 \text{ kg m}^{-3}$ , giving a total  
409 accumulation of 1.85 m w.e. for 2017-18.

410  
411 Based on the above review, we adopt an estimate of  $\bar{a} = 1.8 \pm 0.2$  m w.e.  $\text{yr}^{-1}$  for the net accumulation from 2005 to 2018.  
412 Using this value, the firn layer of Core 1 represents  $12.5 \pm 1.4$  years of net accumulation (i.e., 2005-2017), or  $13.2 \pm 1.4$  years,  
413 if the seasonal snowpack on top is counted. Over 12.5 years, the total measured ice content of 2.67 m w.e. in the firn equates  
414 to an average meltwater refreezing rate of 0.22 m w.e.  $\text{yr}^{-1}$ .

415



#### 418 4.4 Surface energy balance and firn modelling

419 Reconstructed air temperature, melt, and firn trends from 1965-2019 are shown in Figure 5. Summer air temperature from  
420 the reanalysis (Figure 5A) shows a modest but statistically significant increase over the study period, with a trend of  $+0.07^{\circ}\text{C}$   
421  $\text{decade}^{-1}$ . Table 2 reports changes in meteorological, energy balance, and modelled firn conditions over this time. Specific  
422 humidity and incoming longwave radiation increase markedly over the 55 years, with trends of  $+0.1 \text{ g kg}^{-1} \text{ decade}^{-1}$  and  $+3.5$   
423  $\text{W m}^{-2} \text{ decade}^{-1}$ , respectively. This echoes the findings of Williamson et al. (2020), who report decadal-scale, high-elevation  
424 warming in the St. Elias Mountains in association with increases in atmospheric water vapour and longwave radiation. These  
425 trends augment the net energy available for melt, through increases in both the net radiation and latent heat flux. Modelled  
426 annual melt averaged  $230 \pm 210 \text{ mm w.e. yr}^{-1}$  from 1965 to 2019 and  $380 \pm 310 \text{ mm w.e. yr}^{-1}$  from 2005 to 2017, 70% higher  
427 than the long-term average. The latter interval represents the approximate period of record of the firn core. The trend in  
428 surface melting is  $+62 \text{ mm w.e. yr}^{-1} \text{ decade}^{-1}$  from 1965 to 2019 (Figure 5B). The summer of 2013 was exceptional; it had  
429 the warmest summer temperatures on record,  $T_{JJA} = -0.7^{\circ}\text{C}$ , with 895 mm w.e. of meltwater (Table 2).

430  
431 Within the model, 91% of the surface meltwater refreezes in the firn over the period 1965-2019, with 100% of it refreezing  
432 in cool summers when meltwater generation is limited. Meltwater that does not refreeze percolates to depth in the firn  
433 model. Figure 5B plots the annual melting minus refreezing, with positive values indicating deep percolation. If the firn is  
434 temperate ( $0^{\circ}\text{C}$ ), meltwater can percolate through the entire depth of the firn column (35 m), where it is permitted to “drain”  
435 through the lowest layer; this water leaves the system and is considered as runoff. Porewater in the firn can also refreeze in  
436 the subsequent winter, to the depth of the winter cold wave ( $\sim 8 \text{ m}$ ), accounting for the negative values in Figure 5B. This is  
437 percolated meltwater that refreezes within the firn column in the following calendar year. Complete meltwater retention is  
438 typical for most of the period from 1965 to the early 2010s, but there is a marked increase in modelled runoff over the last  
439 decade (Figure 5B), indicating drainage through the full 35-m firn column. Only 72% of the surface melt refroze during the  
440 period 2005-2017, with a five-fold increase in meltwater drainage, from an average of  $-20 \pm 120 \text{ mm w.e. yr}^{-1}$  from 1965-  
441 2019 to  $-105 \pm 220 \text{ mm w.e. yr}^{-1}$  from 2005-2017. Meltwater that drains to the deep firn is partitioned between porewater  
442 storage (meltwater retention) and deep drainage (mass loss). This partitioning was almost equal in the firn model over the  
443 period 2005-2017, with an average of 52 mm w.e.  $\text{yr}^{-1}$  stored as liquid water in the deep firn and 54 mm w.e.  $\text{yr}^{-1}$  of runoff:  
444 water that drains out through the bottom layer of the firn, leaving the system. This equates to a total meltwater retention of  
445 86% as either liquid water or refrozen ice, with a mass loss representing 14% of the summer melt.

446  
447 Summers with high amounts of surface melt produce greater refreezing and warming of the snow and firn, eventually  
448 overwhelming the content and enabling deep percolation and drainage. Figures 5C and 5D plot the modelled evolution of the  
449 firn temperatures and the wetting and melting fronts, which closely coincide. Snow and firn temperatures in Figure 5C are  
450 mean annual values at the snow surface (the upper 0.1 m), and at 10, 20, and 35 m depth. For a purely conductive

Shawn Marshall 3/10/2021 11:16 AM

Deleted: s

Shawn Marshall 3/10/2021 11:16 AM

Deleted: represents

Shawn Marshall 3/10/2021 11:17 AM

Deleted: 73

Shawn Marshall 3/10/2021 11:18 AM

Deleted: and the mass loss associated with summer mass balance increased

Naomi Ochwat 3/10/2021 8:59 PM

Deleted: cold

457 environment, ~10 m represents the depth of the annual temperature wave (Cuffey and Paterson, 2010), but latent heat release  
458 from meltwater refreezing warms the subsurface and causes a deeper influence of surface conditions, such that 10-m  
459 temperatures are highly variable (Table 2). The modelled wetting and melting fronts in Figure 5D suggest dramatic recent  
460 developments in firn thermal and hydrological structure at the Kaskawulsh drill site, with a regime shift in the firn structure  
461 over the period 2013-2017. This is consistent with the birth of a deep PFA at this time. Figure 6 plots the full subsurface  
462 temperature evolution over the period 1965-2019, showing the typical seasonal evolution of firn temperatures and the  
463 unusual nature of the hydrological breakthrough event that began in 2013 and persists through 2019. Figures 5E and 5F plot  
464 the modelled increases in average firn density and total firn ice content from 1965-2019. The average firn density in the  
465 model is  $682 \text{ kg m}^{-3}$  in 2018, compared with  $698 \pm 5 \text{ kg m}^{-3}$  measured in Core 1. The modelled firn densification since the  
466 1960s roughly matches the observed density trend.

467  
468 The model results in Figures 5 and 6 are for the 'reference' 1965-2019 ERA climatological forcing and firn model  
469 parameters. These are the direct ERA climate fields, bias-adjusted to represent the elevation of the core site and to give  
470 consistency with the regional Copland weather station data (2014-2018). The weather station has a similar elevation and  
471 topoclimatic environment and is about 11 km from the core site, falling within the same ERA5 grid cell. Firn model settings  
472 are based on calibrations against field data at DYE-2, Greenland, within the percolation zone of the southern Greenland Ice  
473 Sheet (Samimi et al., 2020), but we have no local field calibration of these model parameters. There are therefore  
474 uncertainties within both the climate forcing and the model parameters and assumptions. The Supplemental Information  
475 examines the sensitivity of model results to several important meteorological inputs and model parameters, as well as the  
476 strategy adopted for the model spin-up.

477  
478 Selected results of the sensitivity tests are plotted in Figure 7, indicating the wide range of model behaviour that is possible  
479 with perturbations to the model inputs, parameter settings, and spin-up assumptions. An air temperature anomaly of  $\pm 1^\circ\text{C}$   
480 applied to the reference ERA climatology gives very different firn evolutions from 1965-2019, with warmer temperatures  
481 driving a shift to temperate firn conditions in the late 1980s (Figures 7A and C). Warming of  $2^\circ\text{C}$  gives temperate firn for the  
482 entire period. In the other direction, a temperature anomaly of  $-1^\circ\text{C}$  is sufficient to maintain polythermal conditions at the  
483 site, precluding the development of deep temperate firn or a PFA. Similar results are obtained with perturbations of  $\pm 10 \text{ W}$   
484  $\text{m}^{-2}$  to the incoming longwave radiation (Supplemental Information). Increases in meltwater infiltration that are stimulated by  
485 lower values of the irreducible water content ( $\theta_{ir} < 0.025$ ) have a similar effect to warming, promoting meltwater infiltration,  
486 firn warming, and the earlier development of temperate firn.

487  
488 The simulations are also sensitive to the initial conditions (Figures 7B and D). Given evidence from Grew and Mellor (1966)  
489 that firn at 15-m depth was temperate in the mid-1960s near our core site, we introduce temperature anomalies from  $+0.5$  to

Shawn Marshall 3/10/2021 11:27 AM

Deleted: to

Shawn Marshall 3/10/2021 11:27 AM

Deleted: and roughly matches the observed density trend.

Naomi Ochwat 3/6/2021 6:57 PM

Deleted: perpetual

Naomi Ochwat 3/6/2021 6:32 PM

Deleted: attained

495 +2°C to the spin-up climatology. A perturbation of +1.5°C creates temperate conditions to 12-m depth, and +2°C is  
496 sufficient to create deep temperate firm which persists for several years (Figure 7D). Firm refreezes in the 1970s within the  
497 model, and eventually follows a similar path to the reference simulation, but with a memory of warmer initial firm  
498 temperatures. This permits a more rapid transition (or return) to deep temperate conditions spurred by the heavy melt season  
499 in 2013. Overall, the model sensitivities in Figure 7 indicate that a wide range of model solutions is possible at this site,  
500 indicating that Kaskawulsh Glacier firm is very close to the threshold for either temperate or polythermal conditions. We  
501 discuss this further below.

502  
503 The temperature forcing required to induce temperate firm the 1960s is relatively strong. The year 1965 that is used for the  
504 model initialization is representative of the long-term mean climatology of the site, with mean summer and annual air  
505 temperatures of -2.5°C and -10.8°C. This compares with averages of  $-2.4 \pm 0.8^\circ\text{C}$  and  $-10.7 \pm 0.9^\circ\text{C}$  for the period 1965-  
506 2019 (Table 2). Incoming solar and longwave radiation in summer, 1965 averaged 304 and 240  $\text{W m}^{-2}$ , compared with long-  
507 term averages of 298 and 255  $\text{W m}^{-2}$ . Net energy and melt were slightly lower than the long-term average, due to low  
508 incoming longwave radiation, but overall, 1965 was a typical year. A warm anomaly of +2°C represents 2.5 standard  
509 deviations above normal, giving a mean summer temperature of -0.5°C; this would represent the warmest summer on  
510 record.

511  
512 The initial firm density and ice content are relatively high when we force the model to produce temperate firm conditions in  
513 the mid-1960s through the +2°C air temperature anomaly in the model spin-up. Values in 1965 are 679  $\text{kg m}^{-3}$  and 2.8 m,  
514 compared with reference model values of 641  $\text{kg m}^{-3}$  and 0.7 m. Figure 8 plots the subsequent firm temperature and density  
515 evolution if the +2°C temperature anomaly is maintained from 1965 to 2019 and in the case where the model forcing is  
516 restored to the reference ERA climatology from 1965 to 2019. Subsurface temperature and density evolutions in the latter  
517 case parallel that of the reference model after a transient adjustment period of about a decade, while the perpetual +2°C  
518 anomaly maintains dense and temperate firm. The decadal adjustment of firm density (Figure 8B) is the 'over-turning' time of  
519 the firm core, for downward advection of new snow and firm to 35 m depth. The temperature adjustment (Figures 8A,C) does  
520 not follow this as it is governed by thermal diffusion time scales in the deep firm, giving a longer memory of the initial  
521 conditions.

522

- Shawn Marshall 3/10/2021 11:56 AM  
Formatted: Font color: Text 1
- Shawn Marshall 3/10/2021 11:56 AM  
Formatted: Font color: Text 1
- Shawn Marshall 3/10/2021 11:56 AM  
Formatted: Font color: Text 1
- Shawn Marshall 3/10/2021 11:56 AM  
Formatted: Font color: Text 1
- Shawn Marshall 3/10/2021 11:56 AM  
Formatted: Font color: Text 1
- Shawn Marshall 3/10/2021 11:56 AM  
Formatted: Font color: Text 1
- Shawn Marshall 3/10/2021 11:56 AM  
Formatted: Font color: Text 1
- Shawn Marshall 3/10/2021 11:56 AM  
Formatted: Font color: Text 1
- Shawn Marshall 3/10/2021 11:56 AM  
Formatted: Font color: Text 1
- Shawn Marshall 3/10/2021 11:56 AM  
Formatted: Font color: Text 1
- Shawn Marshall 3/10/2021 12:07 PM  
Formatted: Font:5 pt
- Naomi Ochwat 3/10/2021 8:59 PM  
Deleted:
- Shawn Marshall 3/10/2021 11:56 AM  
Formatted: Font color: Text 1
- Shawn Marshall 3/10/2021 11:56 AM  
Formatted: Font color: Text 1
- Shawn Marshall 3/10/2021 11:56 AM  
Formatted: Font color: Text 1
- Shawn Marshall 3/10/2021 11:56 AM  
Formatted: Font color: Text 1
- Shawn Marshall 3/10/2021 11:56 AM  
Formatted: Font color: Text 1
- Shawn Marshall 3/10/2021 12:02 PM  
Deleted: an
- Shawn Marshall 3/10/2021 12:03 PM  
Deleted: of
- Shawn Marshall 3/10/2021 12:02 PM  
Deleted: +2°C i

528 **5.1 Firn characteristics and changes over time**

529 The accumulation area of Kaskawulsh Glacier currently has indications of widespread meltwater percolation and refreezing.  
 530 Meltwater is stored within the firn as ice, as indicated by the presence of ice layers and infiltration ice, and there is liquid  
 531 water at a depth of ~35 m below the surface. The density of the firn has increased by about 15% since 1964 in the first 7 m  
 532 of firn, due to the increased presence of ice layers. However, the firn in 1964 was not without meltwater percolation and  
 533 refreezing; Grew and Mellor (1966) note the presence of refrozen ice lenses and glands and report evidence for meltwater  
 534 infiltration and refreezing at depths of ~5 m. Nevertheless, the quantity and thickness of ice layers and lenses have increased  
 535 towards present day, as reflected in the changes in the stratigraphy and the density (Figure 4). The firn modelling also  
 536 indicates decadal-scale increases in firn ice content and density (Table 2, Figure 5E). For the reference model parameter  
 537 settings and ERA climate forcing, the model predicts a significant increase in melting (Figure 5B), driving increases in the  
 538 depth of the melting and wetting fronts, meltwater percolation and runoff, and latent heat release associated with refreezing  
 539 since the 1960s. This fundamentally changes the way the firn contributes to the mass balance of the glacier and englacial  
 540 hydrological dynamics, as discussed further in section 5.3. There are significant decadal firn warming trends in the model  
 541 (Figures 5 and 6), driven by the increases in melting and meltwater percolation. The modelling is not observationally  
 542 constrained, however (Figure 7 and Supplementary Material), so the simulated firn warming is uncertain.

543  
 544 Increased firn meltwater and ice content, as well as potential firn warming in recent decades, will affect firn densification  
 545 processes. Melting rounds snow grains and increases the rate of the first stage of densification. With enough melt to drive  
 546 meltwater percolation through the snow and firn layer, meltwater can fill in air pockets and refreeze, further accelerating the  
 547 transition from snow to ice (Cuffey and Paterson, 2010). The overall pattern of density measurements from 2018 resembles a  
 548 logarithmic densification curve (Figure 2), as is typical for Sorge's Law of densification in dry snow (Sorge, 1935, Bader,  
 549 1954). However, with increasing meltwater percolation and refreezing effects, higher densities are common in the upper  
 550 portions of the firn, as observed in our cores. Bezeau et al. (2013) report similar findings from Devon Ice Cap, where they  
 551 found a depth-density reversal and suggest that Sorge's Law no longer holds in areas of significant warming. To account for  
 552 this, firn densification models are being revised to address the effects of ice layers and warming temperatures on the rate of  
 553 densification (Reeh, 2008; Ligtenberg et al., 2011), and other studies are revising mass balance estimates based on dynamic  
 554 densification rates (e.g., Schaffer et al., 2020).

556 **5.2 Perennial Firn Aquifer**

557 We found unequivocal evidence for a deep perennial firn aquifer on the Upper Kaskawulsh Glacier, with excess water in the  
 558 firn pore space below about 32 m depth. Some of this water drained during firn core acquisition (Supplemental material  
 559 video 1 & 2, <https://doi.org/10.5446/50918> and <https://doi.org/10.5446/50919>, respectively). We cannot tell whether this

Naomi Ochwat 3/10/2021 6:09 PM

Deleted: (Cuffey and Paterson, 2010),

Luke Copland 3/8/2021 11:48 AM

Deleted: the

562 PFA is a new feature at this site. Borehole temperature measurements from 1964 at a site close to our cores indicate  
563 temperate conditions at 15-m depth at this time (Grew and Mellor, 1966), and it is possible that firn has been temperate since  
564 that time, conducive to a PFA below the depth of the annual winter cold wave. There are no historical temperature  
565 measurements from greater firn depths at the site, and earlier coring efforts and radar surveys from the upper Kaskawulsh,  
566 Divide, or Eclipse sites make no comment or inference about the presence of liquid water, so we cannot attest to the age or  
567 origins of the PFA. It may well be a new feature.

568  
569 The modelling results suggest that there are significant decadal increases in melting and refreezing since the 1960s at this  
570 site, driving firn warming, increased ice content, and densification (Table 2). The firn model predicts the development of  
571 wet, temperate conditions in the deep firn following the 2013 melt season, although it takes four years to fully develop  
572 (Figure 6). This was triggered by meltwater penetration to 11 m depth in 2013, which is below the depth of penetration of the  
573 winter cold wave. Temperate conditions propagated downwards in the following years and persisted to 2019, supported by  
574 several more years with above-average melting. Deep meltwater percolation during these years would support the  
575 development and recharge of a PFA or perched water table at the glacier ice-firn interface. This agrees with the stratigraphy  
576 found in the field. The presence of firn that has not been visibly affected by meltwater overlying the PFA implies that deep  
577 meltwater infiltration through vertical piping may be an important process here and may allow the PFA to be recharged in a  
578 heavy melt season. In the model, deep recharge does not occur every summer after the establishment of a temperate firn  
579 column; the summer melt still needs to break through the winter cold layer, which typically extends to 6-7 m depth (Figure  
580 6). Also of interest in Figure 6 is a large melt event in 2007, which led to meltwater infiltration and warming to about 9-m  
581 depth. This was similar to the 2013 melt event, but the summers of 2008 to 2010 were relatively cool (average JJA  
582 temperatures of  $-2.8^{\circ}\text{C}$  and melting of 111 mm w.e.), leading to refreezing in the upper 9 m of firn. Thawing of the full 35-  
583 m firn column to shift it from polythermal to temperate conditions requires several years of sustained melt forcing in the  
584 model.

585  
586 There are significant uncertainties in the modelling, associated with the climatological forcing, surface energy balance and  
587 firn model parameterizations, and initial conditions. The Supplemental Information explores these in detail, while Figure 7  
588 provides an illustration of the range of simulated behaviour for different model settings. The 'reference model' results  
589 presented in Figures 5 and 6 should be seen as just one scenario, corresponding to our best estimate of the parameter settings.  
590 We lack local calibration and validation studies, so we cannot preclude different firn temperature and melt evolutions at this  
591 site, particularly given the inference of Grew and Mellor (1966) that firn at 15-m depth was temperate in the mid-1960s. The  
592 default model parameters and spin-up settings do not produce this; augmented warming or incoming radiation fluxes need to  
593 be introduced to the ERA climatology to produce temperate firn at this time. It is possible that strong melt seasons in the  
594 early 1960s created temporary temperate conditions in the upper firn column. Alternatively, the surface energy balance and  
595 firn hydrological models may underestimate the amount of melting and meltwater infiltration. The one firn conclusion is

596 that the climatological and glaciological conditions on the upper Kaskawulsh Glacier are very close to the tipping point  
597 between polythermal and temperate conditions. A slight nudge to either side of the reference model settings can give either  
598 persistently sub-zero or persistently thawed conditions in the deep firn at this site (Figures 7 and S1).

599

600 The presence of the deep PFA in 2018 indicates that it is currently temperate, despite mean annual air temperatures of about  
601  $-11^{\circ}\text{C}$ . Meltwater refreezing releases enough latent heat to bring the firn to  $0^{\circ}\text{C}$ . All model simulations concur on this,  
602 although the long-term evolution is uncertain. We don't know the fate of the water that drains through the firn, but the  
603 reference model predicts a total drainage of 1.13 m w.e. over the 55-year simulation, most of this over the last decade. Some  
604 of this is retained within the PFA, but some can be expected to run off. The water in the PFA on Kaskawulsh Glacier is  
605 likely to be flowing, redistributing mass. The drill site was located high in the glacier's accumulation zone, with a gently  
606 sloping surface ( $< 0.6^{\circ}$ ) resulting in a subtle hydraulic gradient. We likely drilled into the top of the water table of the PFA,  
607 and with densities near the pore close-off density, it is likely the PFA does not extend much deeper. There may be  
608 downslope flow along the firn-ice interface, as well as possible Darcian flow within the PFA itself (e.g., Christianson et al.,  
609 2015).

610

611 The liquid-phase meltwater retention on Kaskawulsh is similar to the PFAs found in the high-accumulation areas of southern  
612 Greenland and Svalbard (e.g., Miège et al., 2016; Christianson et al., 2015), and different than the water-saturated layers  
613 commonly found on temperate glaciers. PFAs that have been studied on temperate mountain glaciers typically have a  
614 saturated layer close to the surface (for example, 5 m below the surface at Storglaciären), have active discharge and recharge  
615 processes (Fountain and Walder, 1998; Schneider, 1999; Glazyrin et al., 1977), and appear to experience seasonal drainage  
616 over the winter months (Fountain, 1989, 1996; Jansson et al., 2003), likely due to high hydraulic gradients. Active water  
617 flow in the firn has been observed in 19-m and 25-m pits at Abramov Glacier (Glazyrin et al., 1977), as well as Austfonna  
618 ice cap in 1985 at 7 m depth where they also found sub-horizontal melt channels at 7, 15, and 30 m (Zagorodnov et al.,  
619 2006). In 2012, "water-saturated" firn was found at 40-m depth in an ice core from Mt. Waddington, British Columbia (Neff  
620 et al., 2012). However, they reported no significant alteration of chemistry from the melt above this layer and no additional  
621 analysis of this layer was discussed (Neff et al., 2012). In 2015, a PFA was found on Holtedahlfonna icefield in Northwest  
622 Svalbard (Christianson et al., 2015), and in 2019 a PFA was investigated at Lomonosovfonna ice cap approximately 100 km  
623 to the southeast (Hawrylak and Nilsson, 2019).

624

625 According to Kuipers Munneke et al. (2014), PFA formation in Greenland is contingent upon a high annual snow  
626 accumulation, which helps to insulate the underlying firn from the winter cold wave. Mean annual temperatures in  
627 Greenland are well below  $0^{\circ}\text{C}$  and PFAs require latent heat release from meltwater refreezing, to warm the snow and firn to  
628  $0^{\circ}\text{C}$ , along with meltwater penetration to depths of at least 10 m, to evade the winter cold wave (Kuipers Munneke et al.,  
629 2014). The firn modelling suggests that meltwater penetration to depths of 10 m is rare at Kaskawulsh Glacier, but can occur

Luke Copland 3/8/2021 11:53 AM

Deleted: -

Luke Copland 3/8/2021 11:53 AM

Deleted:

632 in strong melt seasons. Based on our measurements and earlier reports from the IRRP (Wood, 1963; Grew and Mellor,  
633 1966), the estimated accumulation rate at our study site is 1.8 m w.e. yr<sup>-1</sup>. This is similar to reported accumulation rates  
634 where PFAs have been identified in southeastern Greenland (e.g., Miège et al., 2016). Melt rates at southeast Greenland PFA  
635 locations are also comparable to those on the upper Kaskawulsh. Miège et al. (2016) report 0.73 m w.e. yr<sup>-1</sup> over the time  
636 period 1979-2014, while Miller et al. (2020) estimated annual melt rates from 0.24-0.50 m w.e. yr<sup>-1</sup> in a PFA field study at  
637 1700 m elevation in the Helheim Glacier catchment. Modelled melt rates on the upper Kaskawulsh Glacier are estimated at  
638 0.52±0.27 m w.e. yr<sup>-1</sup> from 1965-2019 (Table 2). Recent (2005-2017) Kaskawulsh melt rates increased to 0.72 ± 0.38 m  
639 w.e. yr<sup>-1</sup>, similar to the long-term estimate of Miège et al. (2016) in southeast Greenland, and perhaps close to the threshold  
640 for PFA formation and recharge.

### 641 5.3 Implications for geodetic mass balance

642 Liquid water is commonly found in the temperate firm of low- and mid- latitude mountain glaciers and plays an important  
643 role in meltwater storage and glacier hydrology and mass balance (Fountain and Walder, 1989; Schneider, 1999). For  
644 example, storage of meltwater in a PFA accounts for as much as 64% of internal accumulation for glaciers in Alaska and  
645 Sweden (Trabant and Mayo, 1985; Schneider and Jansson, 2004). In general, melt can result in net surface lowering in four  
646 main ways, but with differing impacts on mass balance: (i) melt which runs off results in direct mass loss; (ii) melt which  
647 percolates and refreezes internally can result in surface lowering, with little to no mass loss; (iii) melt which makes it into a  
648 PFA likely contributes to mass loss, but the storage of liquid water at the firm-ice interface delays runoff from hours to weeks  
649 or longer (Jansson et al., 2003), and (iv) accelerated compaction of warming firm can result in accelerated surface lowering,  
650 without any mass loss. These components can be interrelated and their relative importance depends on many factors  
651 including spatial and temporal variations in melt, PFA thickness, the presence of ice lenses, and firm temperature, so their  
652 effects are difficult to disentangle. We provide further information about these components below, including an assessment  
653 of their relative importance for Kaskawulsh Glacier.

654 x  
655 The climate reanalysis suggests that the effects of meltwater storage through refreezing or liquid retention are increasing as  
656 the climate is warming. Geodetic mass balance measurements are compromised by climate change-induced densification  
657 changes that are not accounted for when interpreting surface lowering of the accumulation zone (Reeh, 2008; Huss, 2013).  
658 Mass balance studies in Greenland indicate that changing melt regimes, meltwater refreezing, and the unknown density and  
659 pore capacity of snow and firm pose significant uncertainties when modelling the surface mass balance of ice sheets  
660 (Lenaerts et al., 2019). Meltwater retention as porewater or refrozen ice will delay surface runoff, dependent on the water  
661 storage characteristics of firm (e.g., pore space availability, water at interstitial grain boundaries) (Fountain and Walder,  
662 1989; Schneider, 1999). If ice layers become too extensive or thick, they can form an 'ice slab,' a thick impermeable barrier  
663 that leads to enhanced surface runoff (MacFerrin et al., 2019). The thickness of ice layers that prevents percolation is not  
664 well understood. For example, in Greenland 12-cm thick ice layers were still permeable (Samimi et al., 2020) whereas Bell

Luke Copland 3/8/2021 2:38 PM

**Deleted:** The solid and liquid phase storage mechanisms in the Kaskawulsh Glacier firm layer have different implications for the mass balance of the glacier.

Luke Copland 3/8/2021 2:44 PM

**Moved (insertion) [1]**

Luke Copland 3/8/2021 2:54 PM

**Deleted:** This melt can account for as much as 64% of internal accumulation, as found in Alaska and Sweden (Trabant and Mayo, 1985; Schneider and Jansson, 2004).

Luke Copland 3/8/2021 2:51 PM

**Deleted:** Liquid water is commonly found in the temperate firm of low- and mid- latitude mountain glaciers and has played an important role in meltwater storage and glacier hydrology (Fountain and Walder, 1989; Schneider, 1999). Depending on the melt, PFA thickness, and temperature of the firm, the storage of liquid water at the firm-ice interface delays runoff from hours to weeks or longer (Jansson et al., 2003). This melt can account for as much as 64% of internal accumulation, as found in Alaska and Sweden (Trabant and Mayo, 1985; Schneider and Jansson, 2004).

Luke Copland 3/8/2021 2:44 PM

**Moved up [1]:** the storage of liquid water at the delays runoff from hours to weeks or longer (Jansson et al., 2003). This melt can account for as much as 64% of internal accumulation, as found in Alaska and Sweden (Trabant and Mayo, 1985; Schneider and Jansson, 2004).

Luke Copland 3/8/2021 2:53 PM

**Deleted:** The effects of meltwater storage through refreezing or liquid retention on high mountain glaciers complicate mass balance measurements.

Luke Copland 3/8/2021 2:53 PM

**Deleted:** se effects

Naomi Ochwat 3/6/2021 6:51 PM

**Deleted:** that causes

Luke Copland 3/8/2021 11:57 AM

**Deleted:** the

Luke Copland 3/8/2021 11:59 AM

**Deleted:** large

698 et al. (2008) reported that a 1-2 cm ice layer prevented percolation at Devon Ice Cap, Canada. These phenomena and effects  
699 are not limited to Greenland and the high Arctic. This study demonstrates that Kaskawulsh Glacier also experiences  
700 meltwater storage in the form of ice layers and liquid water retention (as a PFA), with potentially significant recent changes  
701 in firn structure and meltwater retention capacity. The increases in firn density and ice content found on Kaskawulsh Glacier  
702 appear to be similar to other high-accumulation Arctic regions (Pohjola et al., 2002; De La Peña et al., 2015; Bezeau et al.,  
703 2013).

704  
705 The surface energy balance model is not observationally constrained at this site, so we don't have quantitative confidence in  
706 the modelled mass balance and melt rates, but the reconstructed trends indicate a ~70% increase in summer meltwater  
707 production at this site since the 1960s, leading to increased rates of refreezing and also the onset of meltwater runoff in  
708 recent years. We neglected the potential influence of summer rainfall in this study, as we believe that rain events remain rare  
709 at this site. However, they likely happen from time to time, and could become more prevalent in a warming climate. Rain  
710 events would add sensible heat and liquid water to the snow and firn, further increasing snow and firn temperatures, water  
711 infiltration into the firn, and meltwater runoff, where there is inadequate cold content or pore space to retain this water (as in  
712 recent years at the site). In situ field studies are needed to confirm and constrain the meteorological and energy balance  
713 conditions on the upper Kaskawulsh Glacier, to inform the mass balance processes for both the glacier and the PFA.

714  
715 Melt totals are much less than the annual accumulation (~1.8 m w.e.), so the site remains within the accumulation area of the  
716 glacier, with most of the meltwater refreezing. Increases in meltwater refreezing have driven decadal-scale firn warming  
717 along with increases in ice content and firn density at this site. The modelling suggests a ~5% increase in firn density since  
718 the 1960s and a doubling of the ice content, from 1.1 to 2.3 m over the full 35-m snow/firn column. Increases in summer  
719 melting over the last decade are associated with meltwater infiltration and firn warming in the deep firn, with the likelihood  
720 of meltwater runoff from the site in recent years. Within the model, 91% of surface melt refreezes over the 55-year  
721 simulation, but this declines to 73% for the period 2005-2017. The remaining 27% drains to the deep firn through this  
722 period, where it is either retained within the PFA or it may drain from the system. In the firn model, a total of ~0.7 m of  
723 meltwater is stored as liquid water in the deep firn and ~0.7 m w.e. 'runs off' through the period 2005-2017, draining  
724 through the bottom layer and leaving the system. In reality, this meltwater may drain through lateral transport in the PFA or  
725 at the ice-firn interface.

726  
727 The modelled 2018 firn core has an ice content of 2.6 m, compared to a total ice content of  $2.33 \pm 0.26$  m measured in Core  
728 1. The modelled ice content is a completely independent estimate but is in reasonable agreement with the firn core, giving  
729 some confidence in the modelled refreezing. The model may slightly over-estimate the melt or the meltwater infiltration,  
730 given that the modelled ice content is about 15% too high. However, that inference is not consistent with the apparent cold  
731 bias in the model spin-up. Alternatively, firn in the model may be too cold through much of the simulation, causing an

Luke Copland 3/8/2021 12:00 PM  
Deleted: the

Shawn Marshall 3/10/2021 12:29 PM  
Deleted: well ...uch less than the annual ... [1]

Naomi Ochwat 3/6/2021 7:01 PM  
Deleted: ould also contribute to surface drawdown, as well as mass loss.

Shawn Marshall 3/10/2021 12:56 PM  
Deleted: 96...1% of total meltwater...urfac ... [2]

Luke Copland 3/8/2021 12:02 PM  
Deleted: and

Shawn Marshall 3/8/2021 8:07 PM  
Deleted: , but it is about 15% in excess of the observations. This suggests that t...e model n... [3]



774 overestimate of the modelled meltwater refreezing and retention capacity. If this is the case, runoff (summer mass losses)  
 775 from the site will be higher than our estimates, with negative implications for Kaskawulsh Glacier mass balance.  
 776  
 777 The accumulation zone of Kaskawulsh Glacier is estimated to have experienced a minimum of  $0.73 \pm 0.23$  m of surface  
 778 lowering due to internal refreezing over the period represented by Core 1, which we estimate to be 12.5 years, or  $0.06 \pm 0.02$   
 779  $\text{m yr}^{-1}$  from 2005-2017. This estimate of thinning is likely low, because neither the meltwater retention due to the infiltration  
 780 ice nor the presence of the PFA is included in this estimate. In previous measurements of surface elevation changes on  
 781 Kaskawulsh Glacier, Foy et al. (2011) found that the accumulation zone thinned by an average of  $0.04\text{-}0.11$   $\text{m yr}^{-1}$  from  
 782 1977-2007, with a total thinning of 1–3 m over this period. Larsen et al. (2015) reported mean elevation losses of  $0\text{-}1$   $\text{m yr}^{-1}$   
 783 towards the head of the glacier from 1995-2000. The thinning signal due to meltwater percolation and refreezing is within  
 784 the estimates of Foy et al. (2011) and Larsen et al. (2015), suggesting that some or all of the reported lowering could be due  
 785 to mass redistribution and not mass loss. The density of the firm has increased from 1964-2018 due to meltwater percolation  
 786 and refreezing. It is therefore likely that the surface has lowered since 1964 because of this increased densification.

## 787 6 Conclusion

788 The upper accumulation zone of Kaskawulsh Glacier firm has undergone significant changes since 1964, becoming denser,  
 789 and more ice-rich. The mean density of the first 32 m of firm (4.2 to 36.2 m below the surface) was  $698 \pm 5$   $\text{kg m}^{-3}$ . Analysis  
 790 of historical density data indicate that the firm of Kaskawulsh Glacier has become up to 15% denser since the early 1960s,  
 791 due to the increased ice content and melt-affected firm. Increases in firm density due to meltwater refreezing over the 13-year  
 792 period represented by the firm core (2005-2018) are equivalent to a surface lowering of  $0.73 \pm 0.23$  m ( $0.06 \pm 0.02$   $\text{m yr}^{-1}$ ),  
 793 and this rate of surface lowering is likely increasing in association with the overall densification, connected to increases in  
 794 firm temperature as well as ice content. Though not observationally constrained, and therefore uncertain, the modelling  
 795 results suggest the likelihood of significant increases in melting and refreezing since the 1960s at this site, driving decadal-  
 796 scale increases in firm temperature, ice content, and density. The estimates of firm density and the evidence for densification  
 797 can help to inform geodetic mass balance measurements from this region.

799 Our study also illustrates a high-elevation accumulation area in the St. Elias Mountains that is undergoing a transformation  
 800 in response to climate change. The firm on upper Kaskawulsh Glacier now contains a PFA, which has likely developed over  
 801 the past decade. Firm modelling suggests that the PFA has developed in response to increased summer melting, meltwater  
 802 infiltration, and firm warming from the associated latent heat release. The Kaskawulsh Glacier PFA needs to be more widely  
 803 studied, as the spatial extent and depth of the aquifer are not yet known. Ground-penetrating radar measurements may  
 804 provide a method to investigate the spatial extent of the feature. Use of an electrothermal drill that can drill through water-  
 805 saturated firm may allow estimations of the depth of the firm aquifer, as well as subsequent studies on the potential flow of the

Luke Copland 3/8/2021 12:03 PM  
 Deleted: . The firm has become

Shawn Marshall 3/8/2021 8:18 PM  
 Deleted: warmer,

Shawn Marshall 3/8/2021 8:18 PM  
 Deleted: ,

Luke Copland 3/8/2021 12:04 PM  
 Deleted: since 1964

Shawn Marshall 3/8/2021 8:19 PM  
 Moved down [2]: The firm now contains a PFA, which has likely developed over the past decade.

Shawn Marshall 3/10/2021 1:05 PM  
 Deleted: , and changes in firm densification due to meltwater refreezing into ice layers over the last ~12.5 years (2005-2017) is responsible for an estimated surface lowering of  $0.73 \pm 0.23$  m.

Naomi Ochwat 3/10/2021 6:13 PM  
 Deleted: 12.5

Naomi Ochwat 3/10/2021 6:13 PM  
 Deleted: 7

Shawn Marshall 3/10/2021 1:08 PM  
 Formatted: Font:5 pt

Shawn Marshall 3/10/2021 1:08 PM  
 Formatted: Font:5 pt

Shawn Marshall 3/10/2021 1:18 PM  
 Formatted: Superscript

Shawn Marshall 3/10/2021 1:18 PM  
 Formatted: Superscript

Naomi Ochwat 3/10/2021 9:06 PM  
 Deleted: Thoug

Naomi Ochwat 3/10/2021 9:06 PM  
 Deleted: h

Shawn Marshall 3/8/2021 8:19 PM  
 Moved (insertion) [2]

Shawn Marshall 3/8/2021 8:19 PM  
 Deleted: The

Shawn Marshall 3/8/2021 8:19 PM  
 Deleted: may be a recent feature, attributed

Shawn Marshall 3/8/2021 8:27 PM  
 Deleted: Our study illustrates a high elevation accumulation area that is changing in respons... [4]

Shawn Marshall 3/8/2021 8:29 PM  
 Deleted: . The

Shawn Marshall 3/8/2021 8:29 PM  
 Deleted: is

Shawn Marshall 3/8/2021 8:29 PM  
 Deleted:

838 water within the aquifer. [The firn modelling suggest that this site is experiencing meltwater runoff over the past decade, in](#)  
839 [relation to the development of the PFA. A better understanding of this feature is needed to quantify the extent of meltwater](#)  
840 [retention and the mass balance of Kaskawulsh Glacier.](#) This region will likely continue to experience increasing amounts of  
841 surface melt and refreezing within the snowpack and firn, [extending to higher elevations](#), so there is [some](#) urgency to obtain  
842 climate records from this region.

843

844 *Data availability.* Raw density data is available by contacting the corresponding author.

845

846 *Author contribution.* NO and AC collected field data. AC ran ion analyses, supervised the field campaign and helped with  
847 figures. SM contributed to the design and funding of the study and was responsible for the firn modelling. BM and SM  
848 provided supervision during the project. LC provided weather station data and contributed to the collection and interpretation  
849 of data. NO analysed the data and wrote the manuscript, to which all co-authors contributed.

850

851 *Competing interests.* The authors declare no competing interests.

852

853 *Acknowledgements.* This work was part of a Polar Knowledge Canada Grant in support of Cryosphere-Climate Monitoring at  
854 Kluane Lake Research Station, Yukon Territory. We acknowledge the Natural Sciences and Engineering Research Council  
855 (NSERC) of Canada for additional financial support. We thank Parks Canada for permission to conduct this research in  
856 Kluane National Park, under research and collection permit KLU-2018-28117. We are grateful for the field crew Étienne  
857 Gros and Peter Moraal, Icefield Instruments Inc., for assistance with coring, and members of the University of Ottawa  
858 Glaciology and Northern Field Research classes, particularly Jean Bjornson, for assistance with the snow pit measurements.  
859 The Arctic Institute of North America, Kluane Lake Research Station, and Icefield Discovery supported fieldwork logistics.  
860 We thank Kristina Miller, University of Calgary, for field support and countless glaciological discussions, Shad O’Neel and  
861 Louis Sass of the U.S. Geological Survey for sharing firn density data from Alaska, Christian Zdanowicz, Uppsala  
862 University, for sharing his 2004-2011 snow depth data from the upper Hubbard Glacier, and Eduard Khachatryan for  
863 translating the Glazyrin et al. (1977) paper.

## 864 **References**

865 Bader, H.: Sorge’s law of densification of snow on high polar glaciers, *J. Glaciol.*, 2, 319–323, 1954.

866 Bell, C., Mair, D., Burgess, D., Sharp, M., Demuth, M., Cawkwell, F., Bingham, R. and Wadham, J.: Spatial and temporal  
867 variability in the snowpack of a High Arctic ice cap: implications for mass-change measurements. *Ann. Glaciol.* 48, 159-  
868 170, 2008.

- 869 Berthier, E., Schiefer, E., Clarke, G. K. C., Menounos, B. and Rémy, F: Contribution of Alaskan glaciers to sea-level rise  
870 derived from satellite imagery. *Nat. Geosci.* 3, 92–95, 2010.
- 871 Bezeau, P., Sharp, M., Burgess, D. and Gascon, G: Firm profile changes in response to extreme 21st-century melting at  
872 Devon Ice Cap, Nunavut, Canada. *J. Glaciol.* 59, 981–991, 2013.
- 873 Christianson, K., Kohler, J., Alley, R. B., Nuth, C. and Van Pelt, W. J. J.: Dynamic perennial firn aquifer on an Arctic  
874 glacier. *Geophys. Res. Lett.* 42, 1418–1426, 2015.
- 875 Cogley, J.G.: Geodetic and direct mass-balance measurements: comparison and joint analysis. *Ann. Glaciol.*, 50(50), 96-100,  
876 2009.
- 877 Coleou, C., and Lesaffre, B.: Irreducible water saturation in snow: experimental results in a cold laboratory. *Ann.*  
878 *Glaciol.*, 26, 64–68, <https://doi.org/10.3189/1998AoG26-1-64-68>, 1998.
- 879 Cuffey, K. M., and Paterson, W.: *The Physics of Glaciers* (4th ed.). Boston,; Elsevier. 1-683. 2010.
- 880 De La Peña, S, I. M. Howat, P.W. Nienow, M. R. van den Broeke, E. Mosley-Thompson, S. F. Price, D. Mair, B. Noël, and  
881 A. J. Sole.: Changes in the firn structure of the western Greenland Ice Sheet caused by recent warming. *The Cryosphere*, 9,  
882 1203–1211, 2015.
- 883 Ebrahimi, S. and Marshall, S. J.: Surface energy balance sensitivity to meteorological variability on Haig Glacier, Canadian  
884 Rocky Mountains, *The Cryosphere*, 10, 2799–2819, <https://doi.org/10.5194/tc-10-2799-2016>, 2016.
- 885 Fountain, A. G.: The storage of water in, and hydraulic characteristics of, the firn of South Cascade Glacier, Washington  
886 State, USA. *Ann. Glaciol.*, 13, 69–75. 1989.
- 887 Fountain, A. G.: Effect of Snow and Firn Hydrology on the Physical and Chemical Characteristics of Glacial Runoff.  
888 *Hydrol. Process.* 10, 509–521, 1996.
- 889 Fountain, A. G. and Walder, J. S.: Water flow through temperate glaciers. *Rev. Geophys.*, 36, 299–328. 1998.
- 890 Foy, N., Copland, L., Zdanowicz, C., Demuth, and M., Hopkinson, C.: Recent volume and area changes of Kaskawulsh  
891 Glacier, Yukon, Canada. *J. Glaciol.*, 57, 515–525, <https://doi.org/10.3189/002214311796905596>, 2011.
- 892 Gascon, G., Sharp, M., Burgess, D., Bezeau, P. and Bush, A. B. G.: Changes in accumulation-area firn stratigraphy and  
893 meltwater flow during a period of climate warming: Devon Ice Cap, Nunavut, Canada. *J. Geophys. Res. Earth Surf.* 118,  
894 2380–2391, 2013.
- 895 Grew, E., and Mellor, M.: High snowfields of the St. Elias Mountains, Yukon Territory, Canada. Hanover, N.H. U.S. Army  
896 Materiel Command, Cold Regions Research & Engineering Laboratory Technical Report, 177, 1-26, 1966.
- 897 Glazyrin G.E., Glazyrina E.L., Kislov B.V. and Pertzinger F.I. Water level regime in deep firn pits on Abramov glacier [in  
898 Russian], volume 45. *Gidrometeoizdat*, 2017.
- 899 Harper, J., Humphrey, N., Pfeffer, W. T., Brown, J., and Fettweis, X.: Greenland ice-sheet contribution to sea-level rise  
900 buffered by meltwater storage in firn. *Nature*, 491, 240–243, 2012.

- 901 Harper, J., Humphrey, N., Pfeffer, T. and Brown, J.: Firm Stratigraphy and Temperature to 10 m Depth in the Percolation  
902 Zone of Western Greenland, 2007 – 2009. Institute of Arctic and Alpine Research, University of Colorado, Occasional Paper  
903 60, 2011.
- 904 Hawrylak, M., and Nilsson, E.: Spatial and Temporal Variations in a Perennial Firn Aquifer on Lomonosovfonna, Svalbard.  
905 Uppsala University Independent Project, 2019. <http://www.diva-portal.se/smash/get/diva2:1319193/FULLTEXT01.pdf>.
- 906 Hersbach, H., Bell, B., Berrisford, P. et al.: The ERA5 global reanalysis. Quarterly Journal of the Royal Meteorological  
907 Society, <https://doi.org/10.1002/qj.3803>, 2020.
- 908 Holdsworth, G.: An Examination and Analysis of the Formation of Transverse Crevasses, Kaskawulsh Glacier, Yukon  
909 Territory, Canada. Institute of Polar Studies, 16, 1965.
- 910 Humphrey, N. F., Harper, J. T., and Pfeffer, W. T.: Thermal tracking of meltwater retention in Greenland's accumulation  
911 area. J. Geophys. Res., 117, F01010, <https://doi.org/10.1029/2011JF002083>, 2012.
- 912 Huss, M.: Density assumptions for converting geodetic glacier volume change to mass change, The Cryosphere, 7, 219–244.  
913 2013.
- 914 Jansson, P., Hock, R. and Schneider, T.: The concept of glacier storage: A review. J. Hydrol., 282, 116–129, 2003.
- 915 Koenig, L. S., Miège, C., Forster, R. R. and Brucker, L.: Initial in situ measurements of perennial meltwater storage in the  
916 Greenland firn aquifer. Geophys. Res. Lett. 41, 81–85, 2014.
- 917 Koerner, R. M.: Devon Island Ice Cap: Core Stratigraphy and Paleoclimate. Science, 146, 347–353. 1977.
- 918 Kuipers Munneke, P. K., Ligtenberg, S. R. M., Van Den Broeke, M. R., Van Angelen, J. H. and Forster, R. R.: Explaining  
919 the presence of perennial liquid water bodies in the firn of the Greenland Ice Sheet. Geophys. Res. Lett. 41, 476–483, 2014.
- 920 Larsen, C. F., Burgess, E., Arendt, A. A., O'Neel, S., Johnson, A. J., and Kienholz, C.: Surface melt dominates Alaska  
921 glacier mass balance. Geophys. Res. Lett. 42, 5902–5908. <https://doi.org/10.1002/2015GL064349>, 2015.
- 922 Lenaerts, J. T. M., Medley, B., van den Broeke, M. R. and Wouters, B.: Observing and Modeling Ice Sheet Surface Mass  
923 Balance. Rev. Geophys. 57, 376–420, <https://doi.org/10.1029/2018RG000622>, 2019.
- 924 Ligtenberg, S. R. M., Helsen, M. M., and van den Broeke, M. R.: An improved semi-empirical model for the densification of  
925 Antarctic firn, The Cryosphere, 5, 809–819, doi:10.5194/tc-5-809-2011, 2011.
- 926 Machguth, H., MacFerrin, M., van As, D., Jason E. Box, Charalampos Charalampidis, William Colgan, Robert S. Fausto,  
927 Harro AJ Meijer, Ellen Mosley-Thompson, and Roderik SW van de Wal.: Greenland meltwater storage in firn limited by  
928 near-surface ice formation. Nature Clim Change, 6, 390–393. <https://doi.org/10.1038/nclimate2899>, 2016.
- 929 MacFerrin, M., Machguth H., van As, D. C., Charalampidis, C., C. M. Stevens, C.M., Heilig, A., Vandecrux, B., P. L. Langen,  
930 P. L., Mottram, R., Fettweis, X., van den Broeke, M. R., Pfeffer, W. T., M. S. Moussavi, M. S., and Abdalati. W.: Rapid  
931 expansion of Greenland's low-permeability ice slabs. Nature, 573, 403–407, 2019.
- 932 [Marchenko, S., Pohjola, V.A., Pettersson, R., Van Pelt, W.J., Vega, C.P., Machguth, H., Bøggild, C.E. and Isaksson, E., A  
933 plot-scale study of firn stratigraphy at Lomonosovfonna, Svalbard, using ice cores, borehole video and GPR surveys in  
934 2012–14. J. Glaciol., 63\(237\), 67-78. doi:10.1017/jog.2016.118, 2017.](#)

935 Marcus, M. G. and Ragle, R. H. Snow accumulation in the Icefield Ranges, St. Elias Mountains, Yukon. *Arctic and Alpine*  
936 *Research*, 2(4), 277-292, 1970.

937 Miège, C., Forster, R., Brucker, L., Koenig, L., Solomon, D.K., Paden, J. D., Box, J. E., Burges, E. W., Miller, J. Z.,  
938 McNeerney, L., Brautigam, N., Fausto, R. S., and Gogineni, S.: Spatial extent and temporal variability of Greenland firn  
939 aquifers detected by ground and airborne radars. *J. Geophys. Res. Earth Surf.*, 121, 2381–2398,  
940 <https://doi.org/10.1002/2016JF003869>, 2016.

941  
942 Miller, O., Solomon, D. K., Miège, C., Koenig, L., Forster, R., Schmerr, N. et al. : Hydrology of a perennial firn aquifer in  
943 southeast Greenland: An overview driven by field data. *Water Resources Research*, 56, e2019WR026348. [https://doi.org/](https://doi.org/10.1029/2019WR026348)  
944 [10.1029/2019WR026348](https://doi.org/10.1029/2019WR026348), 2020.

945  
946 Moholdt, G., Nuth, C., Hagen, J. O. and Kohler, J.: Recent elevation changes of Svalbard glaciers derived from ICESat laser  
947 altimetry. *Remote Sens. Environ.*, 114, 2756–2767, 2010a.

948  
949 Moholdt, G., Hagen, J. O., Eiken, T. and Schuler, T. V.: Geometric changes and mass balance of the Austfonna ice cap,  
950 Svalbard. *The Cryosphere*, 4, 21–34, 2010b.

951  
952 Neff, P. D., Steig, Eric J., Clark, Douglas H., McConnell, Joseph R., Pettit, Erin C., and Menounos, Brian.: Ice-core net snow  
953 accumulation and seasonal snow chemistry at a temperate-glacier site: Mount Waddington, southwest British Columbia,  
Canada. *J. Glaciol.* 58(212), 1165-1175. <https://doi.org/10.3189/2012JoG12J078>, 2012.

954  
955 Noël, B., van de Berg, W.J., Lhermitte, S., Wouters, B., Schaffer, N. and van den Broeke, M.R., 2018. Six decades of glacial  
956 mass loss in the Canadian Arctic Archipelago. *J. Geophys. Res. Earth Surf.*, 123(6), 1430-1449.  
<https://doi.org/10.1029/2017JF004304>, 2018.

957  
958 Noël, B., Jakobs, C.L., van Pelt, W.J.J., Lhermitte, S., Wouters, B., Kohler, J., Hagen, J.O., Luks, B., Reijmer, C.H., Van de  
959 Berg, W.J. and van den Broeke, M.R.: Low elevation of Svalbard glaciers drives high mass loss variability. *Nat Commun.*  
11(1), 1-8. <https://doi.org/10.1038/s41467-020-18356-1> 2020.

960  
961 Parry, V., Nienow, P., Mair, D., Scott, J., Hubbard, B., Steffen, K., and Wingham, D.: Investigations of meltwater refreezing  
962 and density variations in the snowpack and firn within the percolation zone of the Greenland ice sheet. *Ann. Glaciol.* 61–68.  
2007.

963  
964 Pohjola, V. A., Moore, J. C., Isaksson, E., Jauhiainen, T., van de Wal, R. S. W., Martma, T., Meijer, H. A. J., and Vaikmäe,  
965 R.: Effect of periodic melting on geochemical and isotopic signals in an ice core from Lomonosovfonna, Svalbard. *J.*  
*Geophys. Res.*, 107, 4036, 2002.

966  
967 Poli, P., Hersbach, H., Dee, D. P. and 12 others.: ERA-20C: An atmospheric reanalysis of the 20<sup>th</sup> century. *J. Climate*, 29  
(11), 4083-407, <https://doi.org/10.1175/JCLI-D-15-0556.1>, 2016.

968  
969 Reeh, N.: A nonsteady-state firn-densification model for the percolation zone of a glacier, *J. Geophys. Res.*, 113,  
F03023,doi:10.1029/2007JF000746, 2008.

970 Rohatgi, A., WebPlotDigitizer. Version 4.3. 2020. <https://automeris.io/WebPlotDigitizer>

971  
972 Samimi, S. and Marshall, S. J.: Diurnal cycles of meltwater percolation, refreezing, and drainage in the supraglacial  
973 snowpack of Haig Glacier, Canadian Rocky Mountains. *Front. Earth Sci.* 5, 1–15. <https://doi.org/10.3389/feart.2017.00006>,  
2017.

Naomi Ochwat 3/6/2021 6:23 PM

Deleted: ..

975 Samimi, S., Marshall, S. J., and MacFerrin, M.: Meltwater penetration through temperate ice layers in the percolation zone at  
976 DYE-2, Greenland Ice Sheet. *Geophys. Res. Lett.*, 47, e2020GL089211. 2020.

977 Schaffer, N., Copland, L., Zdanowicz, C., Burgess, D., & Nilsson, J.: Revised estimates of recent mass loss rates for Penny  
978 Ice Cap, Baffin Island, based on 2005–2014 elevation changes modified for firn densification. *J. Geophys. Res. Earth Surf.*  
979 125, e2019JF005440. 2020. <https://doi.org/10.1029/2019JF005440>

980 Schneider, T.: Water movement in the firn of Storglaciären. *J. Glaciol.* 45, 286–294, 1999.

981 Schneider, T. & Jansson, P. Internal accumulation in firn and its significance for the mass balance of Storglaciären, Sweden.  
982 *J. Glaciol.* 50, 25–34, 2004.

983 Sorge, E. (1935). Glaziologische Untersuchungen in Eismitte. Wissenschaftliche Ergebnisse der Deutschen Gronland-  
984 Expedition Alfred-Wegener 1929 und 1930-1931, 3, 270. in: K. Wegener, im Auftrag der Notgemeinschaft der Deutschen  
985 Wissenschaft (Ed.), Band III, Glaziologie, 1935.

986 [Sommerfeld, R., and LaChapelle, E.: The classification of snow metamorphism. \*J. Glaciol.\*, 9 \(55\), 3-18.  
987 doi:10.3189/S0022143000026757, 1970.](https://doi.org/10.3189/S0022143000026757)

988

989

990 Trabant, D. C. and Mayo, L. R.: Estimation and effects of internal accumulation on five glaciers in Alaska. *Ann. Glaciol.*, 6,  
991 113–117, 1985.

992 van As, D., Box, J. E., and Fausto, R. S.: Challenges of Quantifying Meltwater Retention in Snow and Firn: An Expert  
993 Elicitation., *Front. Earth Sci.* 4(101), [https://doi: 10.3389/feart.2016.00101](https://doi.org/10.3389/feart.2016.00101), 2016.

994 van Pelt, W., Pohjola, V., Pettersson, R., Marchenko, S., Kohler, J., Luks, B., Hagen, J. O., Schuler, T. V., Dunse, T., Noël,  
995 B., and Reijmer, C.: A long-term dataset of climatic mass balance, snow conditions, and runoff in Svalbard (1957–2018),  
996 *The Cryosphere*, 13, 2259–2280, <https://doi.org/10.5194/tc-13-2259-2019>, 2019.

997 Wagner, P. W.: Description and evolution of snow and ice features and snow surface forms on the Kaskawulsh Glacier.  
998 Icefield Ranges Research Project: Scientific Results, 1, 51-53, 1969.

999 [Vandecrux, B., Mottram, R., Langen, P. L., Fausto, R. S., Olesen, M., Stevens, C. M., Verjans, V., Leeson, A., Ligtenberg,  
1000 S., Kuipers Munneke, P., Marchenko, S., van Pelt, W., Meyer, C. R., Simonsen, S. B., Heilig, A., Samimi, S., Marshall, S.,  
1001 Machguth, H., MacFerrin, M., Niwano, M., Miller, O., Voss, C. I., and Box, J. E.: The firn meltwater Retention Model  
1002 Intercomparison Project \(RetMIP\): evaluation of nine firn models at four weather station sites on the Greenland ice sheet,  
1003 \*The Cryosphere\*, 14, 3785–3810, <https://doi.org/10.5194/tc-14-3785-2020>, 2020.](https://doi.org/10.5194/tc-14-3785-2020)

1004 Vionnet, V., Brun, E., Morin, S., Boone, A., Faroux, S., Le Moigne, P., et al.: The detailed snowpack scheme Crocus and its  
1005 implementation in SURFEX v7.2. *Geosci. Model Dev.* 5, 773–791, doi: 10.5194/gmd-5-773-2012, 2012.

1006 Williamson, S., Zdanowicz, C., Anslow, F., S. Clarke, G. K. C., Copland, L., Danby, R. K., Flowers, G. E., Holdsworth, G.,  
1007 Jarosch, A. H., and Hik, D. S.: Evidence for elevation-dependent warming in the St. Elias Mountains, Yukon, Canada. *J.*  
1008 *Clim.* 3253–3269, [https://doi:10.1175/jcli-d-19-0405.1](https://doi.org/10.1175/jcli-d-19-0405.1), 2020.

1009 Wood, W. A.: The Icefield Ranges Research Project. *Geo. Rev.* 53, 503–529. <https://doi.org/10.1126/science.15.370.195>,  
1010 1963.

- Shawn Marshall 3/9/2021 12:58 PM
- Deleted: -
- Shawn Marshall 3/9/2021 12:59 PM
- Formatted: Font:(Default) +Theme Body
- Shawn Marshall 3/9/2021 12:59 PM
- Formatted: Font:(Default) +Theme Body
- Shawn Marshall 3/9/2021 12:59 PM
- Formatted: Font:(Default) +Theme Body
- Shawn Marshall 3/9/2021 12:59 PM
- Formatted: Font:(Default) +Theme Body
- Shawn Marshall 3/9/2021 12:59 PM
- Formatted: Font:(Default) +Theme Body
- Naomi Ochwat 3/10/2021 6:14 PM
- Formatted: Font:(Default) +Theme Body, Not Italic
- Naomi Ochwat 3/10/2021 6:14 PM
- Formatted: Font:Not Italic
- Naomi Ochwat 3/10/2021 6:14 PM
- Formatted: Font:(Default) +Theme Body
- Shawn Marshall 3/9/2021 12:59 PM
- Formatted: Font:(Default) +Theme Body
- Shawn Marshall 3/9/2021 12:59 PM
- Formatted: Font:(Default) +Theme Body
- Shawn Marshall 3/9/2021 12:58 PM
- Deleted: -
- Shawn Marshall 3/9/2021 12:58 PM
- Formatted: Space After: 0 pt
- Shawn Marshall 3/9/2021 12:57 PM
- Formatted: Font:(Default) +Theme Body

- 1013 Yalcin, K., Wake, C. P., Kreutz, K. J., and Whitlow, S. I.: A 1000-yr record of forest fire activity from Eclipse Icefield,  
1014 Yukon, Canada. *The Holocene*, 16(2), 200–209, <https://doi.org/10.1191/0959683606h1920rp>, 2006.
- 1015 Young, E. M., Flowers, G. E., Berthier, E. and Latto, R.: An imbalancing act: the delayed dynamic response of the  
1016 Kaskawulsh Glacier to sustained mass loss. *Journal of Glaciology*, 18 pp, <https://doi.org/10.1017/jog.2020.107>, 2020.
- 1017 Zagorodnov, V., Nagornov, O., and Thompson, L.: Influence of air temperature on a glacier's active-layer temperature.  
1018 *Annals of Glaciology*, 43, 285-291. doi:10.3189/172756406781812203, 2006.
- 1019 Zdanowicz, C., Smetny-Sowa, A., Fisher, D., Schaffer, N., Copland, L., Eley, J., and Dupont, F.: Summer melt rates on  
1020 Penny Ice Cap, Baffin Island: Past and recent trends and implications for regional climate. *J. Geophys. Res. Earth Surf*, 117,  
1021 F02006, <https://doi.org/10.1029/2011JF002248>, 2012.
- 1022 Zdanowicz, C., Fisher, D., Bourgeois, J., Demuth, M., Sheng, J., Mayewski, P., Kreutz, K., Osterberg, E., Yalcin, K., Wake,  
1023 C., Steig, E., Froese, D., and Goto-Azuma, K.: Ice cores from the St. Elias Mountains, Yukon, Canada: Their significance for  
1024 climate, atmospheric composition and volcanism in the North Pacific region. *Arctic*, 1–23, 2014.
- 1025

1026

1027

1028 **Table 1:** Total ice content, ice fraction ( $F_i$ ), bulk density ( $\rho_b$ ), background density ( $\rho_f$ ), and total water equivalent ( $w$ ), for the  
1029 portion of each core below the last summer surface. Depths are reported from the May 2018 snow surface and the firm  
1030 portion of the core started at the 2017 summer surface, at 4.2 m depth.

1031

	Depth below surface (m)	Total Ice content (m)	$F_i$ (% vol)	$F_i$ (% mass)	$\rho_b$ (kg m <sup>-3</sup> )	$\rho_f$ (kg m <sup>-3</sup> )	$w$ w.e. (m)
Core 1	4.2-14.2	0.67 ± 0.07	6.7 ± 0.7	13.0 ± 1.3	588 ± 8	565 ± 9	5.88 ± 0.08
	4.2-21.6	1.51 ± 0.15	8.7 ± 0.9	15.6 ± 1.6	640 ± 6	613 ± 7	11.08 ± 0.11
	4.2-36.6	2.33 ± 0.26	7.2 ± 0.7	11.9 ± 1.2	698 ± 5	676 ± 6	22.49 ± 0.15
Core 2	4.2-14.2	0.42 ± 0.04	4.2 ± 0.4	8.4 ± 0.8	572 ± 7	556 ± 7	5.72 ± 0.07
	4.2-21.6	0.81 ± 0.08	4.7 ± 0.5	8.5 ± 0.9	624 ± 5	609 ± 6	10.85 ± 0.09
Average	4.2-14.2	1.18	4.0	564	580 ± 5	560 ± 5	5.80 ± 0.05
	4.2-21.6				632 ± 4	611 ± 4	10.97 ± 0.07

1032

1033

Luke Copland 3/8/2021 12:10 PM  
 Deleted: and

Shawn Marshall 3/9/2021 9:44 AM  
 Deleted: content

Shawn Marshall 3/9/2021 9:43 AM  
 Formatted: Font:10 pt, Not Bold

Luke Copland 3/8/2021 12:07 PM  
 Deleted: firm



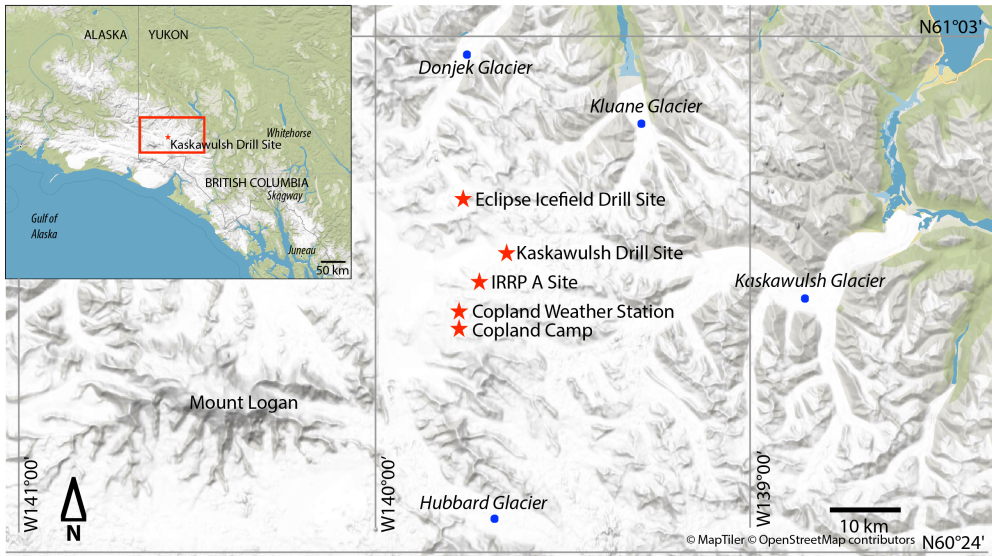
1037  
1038  
1039  
1040  
1041  
1042  
1043  
1044  
1045  
1046  
1047  
1048  
1049  
1050  
1051  
1052  
1053  
1054  
1055  
1056  
1057  
1058  
1059  
1060  
1061  
1062  
1063  
1064  
1065  
1066  
1067  
1068  
1069  
1070  
1071  
1072  
1073  
1074  
1075  
1076  
1077  
1078  
1079  
1080  
1081

**Table 2:** Climate, surface energy balance, and firn conditions, 1965 to 2019, based on the ERA meteorological forcing at the core site. Decadal trends are reported from linear fits to the data. The period 1965-1975 represents the historical baseline period, when much of the work of the IRRP was completed. 2005-2017 represents the period of record of Core 1, and 2013 was an exceptional year, which potentially marked the initial development of the firn aquifer at this site. Melt and refreeze refer to the total annual melting and refreezing in the 35-m snow and firn column, ‘drainage’ is the total annual melt minus refreezing, and ‘net melt’ is the surface mass loss/drawdown associated with summer melting. Freeze-thaw cycles in the surface layer of the snow mean that some fraction of the net energy that is available for melt is directed to refrozen (i.e., recycled) meltwater. As a result, the net melt – meltwater that is available to percolate into the deeper snow- and firn-pack – is less than the total summer melt. Not that rainfall is neglected in this study, and is assumed to be negligible.

	1965-2019 Mean ( $\pm 1 \sigma$ )	Trend (decade <sup>-1</sup> )	1965-1975 Mean ( $\pm 1 \sigma$ )	2005-2017 Mean ( $\pm 1 \sigma$ )	2013
<i>Meteorological Conditions</i>					
$T_{ann}$ (°C)	-10.7 ± 0.9	+0.16	-11.2 ± 0.7	-10.4 ± 1.0	-9.6
$T_{JJA}$ (°C)	-2.4 ± 0.8	+0.07	-2.2 ± 0.9	-2.1 ± 0.7	-0.7
$T_{SJJJ}$ (°C)	-2.3 ± 0.8	+0.29	-2.9 ± 0.9	-1.8 ± 0.6	-0.8
$PDD$ (°C d)	54 ± 23	+3.6	49 ± 16	69 ± 31	123
$q_v$ (g kg <sup>-1</sup> )	3.7 ± 0.2	+0.10	3.5 ± 0.2	3.9 ± 0.2	4.2
<i>Surface Energy Balance (JJA values)</i>					
$Q^*$ (W m <sup>-2</sup> )	18 ± 11	+3.7	8 ± 3	26 ± 13	45
$Q_N$ (W m <sup>-2</sup> )	10 ± 9	+2.6	4 ± 3	16 ± 13	37
net melt (mm w.e. yr <sup>-1</sup> )	230 ± 210	+62	100 ± 80	380 ± 310	895
melt (mm w.e. yr <sup>-1</sup> )	520 ± 270	+81	360 ± 130	720 ± 375	1360
refreeze (mm w.e. yr <sup>-1</sup> )	500 ± 195	+48	360 ± 130	615 ± 205	1100
drainage (mm w.e. yr <sup>-1</sup> )	20 ± 120	+32	0 ± 0	105 ± 215	260
<i>Firn Conditions</i>					
$T_1$ (°C)	-12.8 ± 0.9	+0.2	-13.3 ± 0.8	-12.4 ± 0.9	-11.5
$T_{10}$ (°C)	-7.3 ± 3.4	+1.8	-11.3 ± 0.8	-2.9 ± 2.4	-3.0
$T_{20}$ (°C)	-7.2 ± 3.6	+2.1	-12.2 ± 0.5	-3.7 ± 2.5	-4.5
$T_{35}$ (°C)	-8.0 ± 3.5	+2.1	-12.7 ± 0.4	-4.8 ± 1.9	-5.2
$z_{thaw}$ (m)	6.8 ± 9.4	+3.6	1.2 ± 1.0	13.1 ± 12.5	18.0
$E_{lat}$ (MJ m <sup>-2</sup> )	126 ± 41	+9.3	98 ± 30	147 ± 43	258
$\rho_b$ (kg m <sup>-3</sup> )	655 ± 10	+4.6	645 ± 3	663 ± 12	671
ice content (m)	2.0 ± 0.6	+0.2	1.1 ± 0.3	2.3 ± 0.4	2.6

- Shawn Marshall 3/10/2021 1:58 PM  
**Deleted:** refers to the net surface melting minus refreezing, accounting for meltwater f
- Shawn Marshall 3/9/2021 9:52 AM  
**Deleted:** (. Tthis is the actual surface drawdown associated with summer melting).
- Shawn Marshall 3/8/2021 7:57 PM  
**Formatted:** English (UK)
- Shawn Marshall 3/8/2021 7:57 PM  
**Formatted:** English (UK)
- Shawn Marshall 3/8/2021 7:57 PM  
**Formatted:** English (UK)
- Shawn Marshall 3/8/2021 7:57 PM  
**Formatted:** English (UK)
- Shawn Marshall 3/8/2021 7:57 PM  
**Formatted:** English (UK)
- Shawn Marshall 3/8/2021 7:57 PM  
**Formatted:** English (UK)
- Shawn Marshall 3/8/2021 7:57 PM  
**Formatted:** English (UK)
- Shawn Marshall 3/8/2021 7:57 PM  
**Formatted:** English (UK)
- Shawn Marshall 3/8/2021 7:57 PM  
**Formatted:** English (UK)
- Shawn Marshall 3/8/2021 7:57 PM  
**Formatted:** English (UK)
- Shawn Marshall 3/8/2021 7:57 PM  
**Formatted:** English (UK)
- Shawn Marshall 3/8/2021 7:57 PM  
**Formatted:** English (UK)
- Shawn Marshall 3/8/2021 7:57 PM  
**Formatted:** English (UK)
- Shawn Marshall 3/8/2021 7:57 PM  
**Formatted:** English (UK)
- Shawn Marshall 3/8/2021 7:57 PM  
**Formatted:** English (UK)

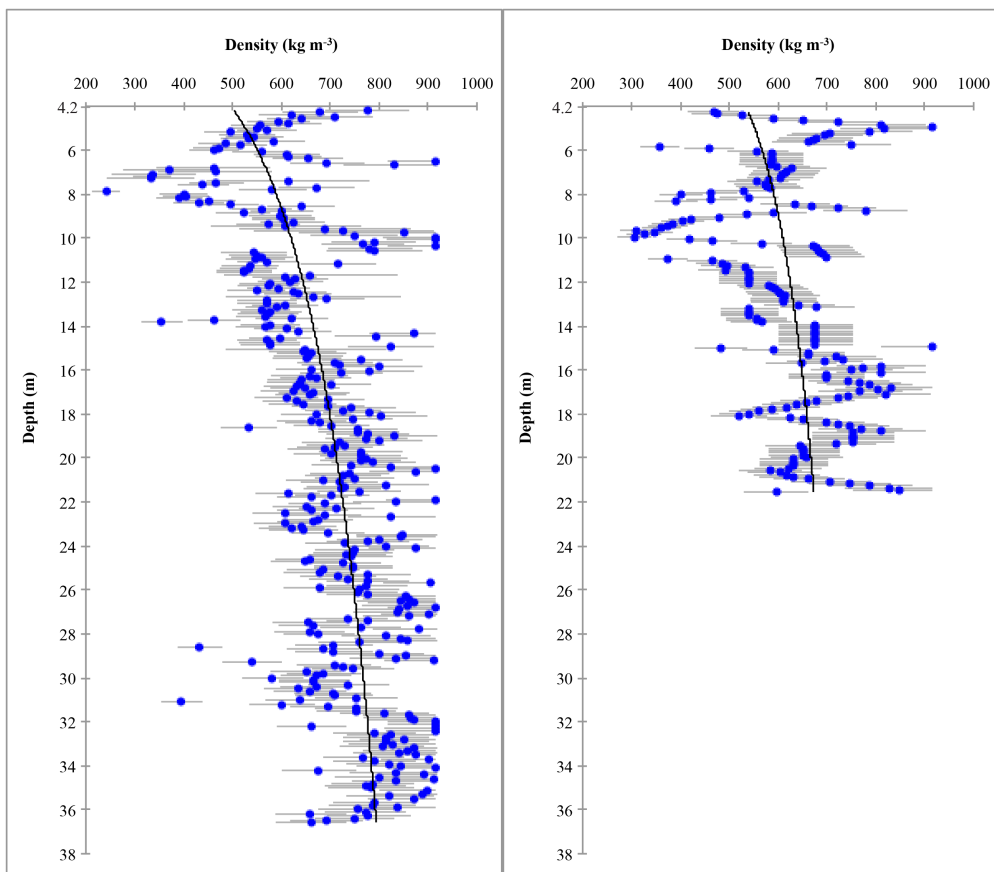
1086



1087

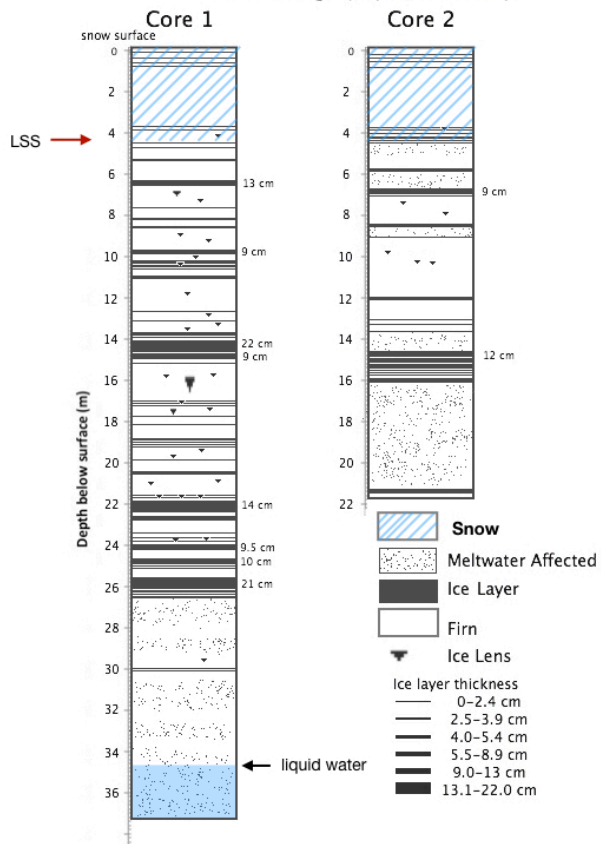
1088

1089 **Figure 1:** Field locations in the St. Elias Icefield, Yukon. IRRP A site is the site of the 1964 firm core that is referenced in  
1090 our study (Grew and Mellor, 1966). Base map from <http://openmaptiles.org/>.



1091  
 1092 **Figure 2:** Measured firn densities of: (A) Core 1, and (B) Core 2 (May 20-24<sup>th</sup> 2018), with uncertainties and best-fit  
 1093 logarithmic curves (black line). The depth scales are truncated at the location of the last summer surface at 4.2 m depth, as  
 1094 the profile consisted of seasonal snow above this.

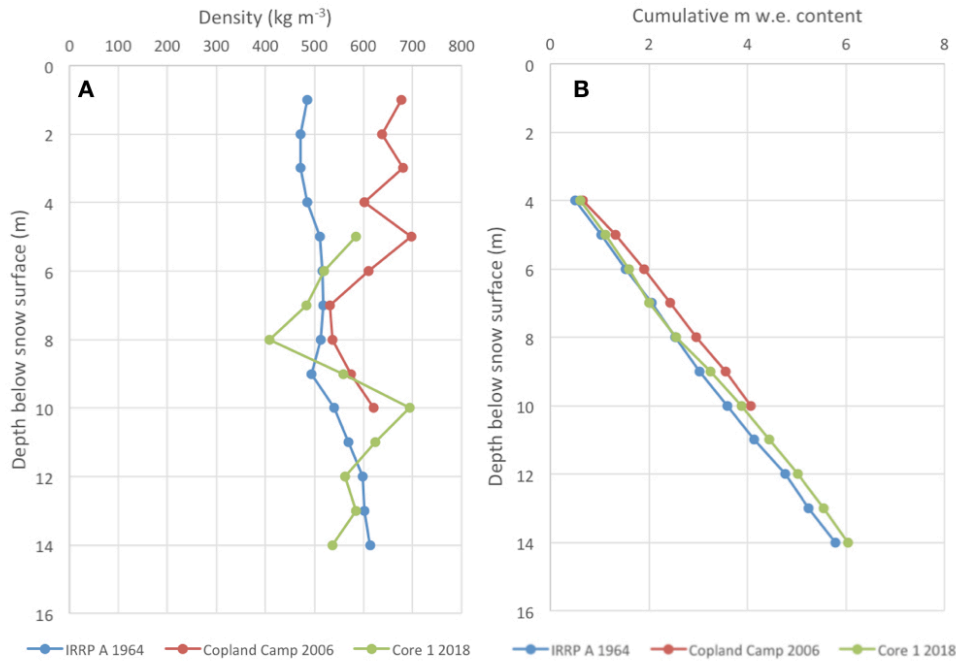
Firn Stratigraphy and Density



1095  
 1096 **Figure 3:** Stratigraphy of the cores collected in May 2018. LSS is the last summer surface [at 4.2 m](#), the boundary between  
 1097 seasonal snow above and firn below. Ice layer thicknesses were classified in the legend by thickness distribution. Note that  
 1098 the ice layers in the first several meters of the core are interpreted as wind crusts.

1099  
 1100  
 1101

1102



1103

1104

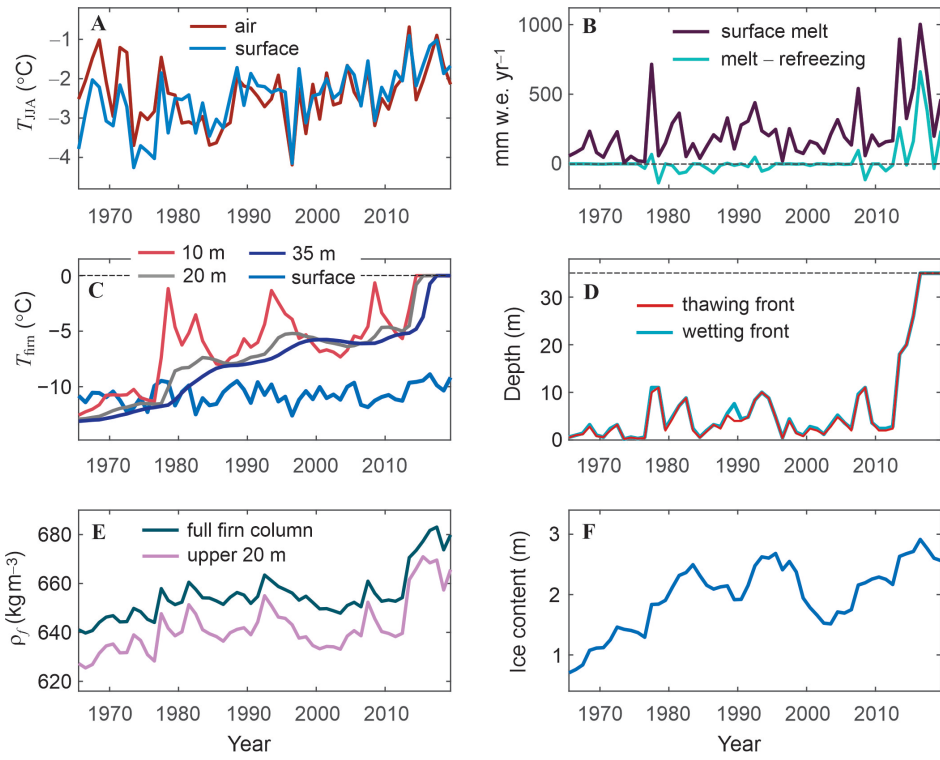
1105 **Figure 4:** A) Comparison of densities averaged over 1 m segments at IRRP A on July 23, 1964 (Grew and Mellor, 1966;  
1106 blue); at Copland Camp on July 14-17, 2006 (red); at Core 1 on May 20-24, 2018 (green). Depth of LSS (i.e., boundary  
1107 between seasonal snow above and firn below) was 3.28 m in 1964, 3.50 m in 2006, and 4.22 m in 2018; the density data for  
1108 2018 begins at the LSS due to the difference in time of year of the measurements compared to the others; B) Comparison  
1109 between cumulative w.e. content in the 1964, 2006 and 2018 profiles, starting at the LSS.

1110

1111

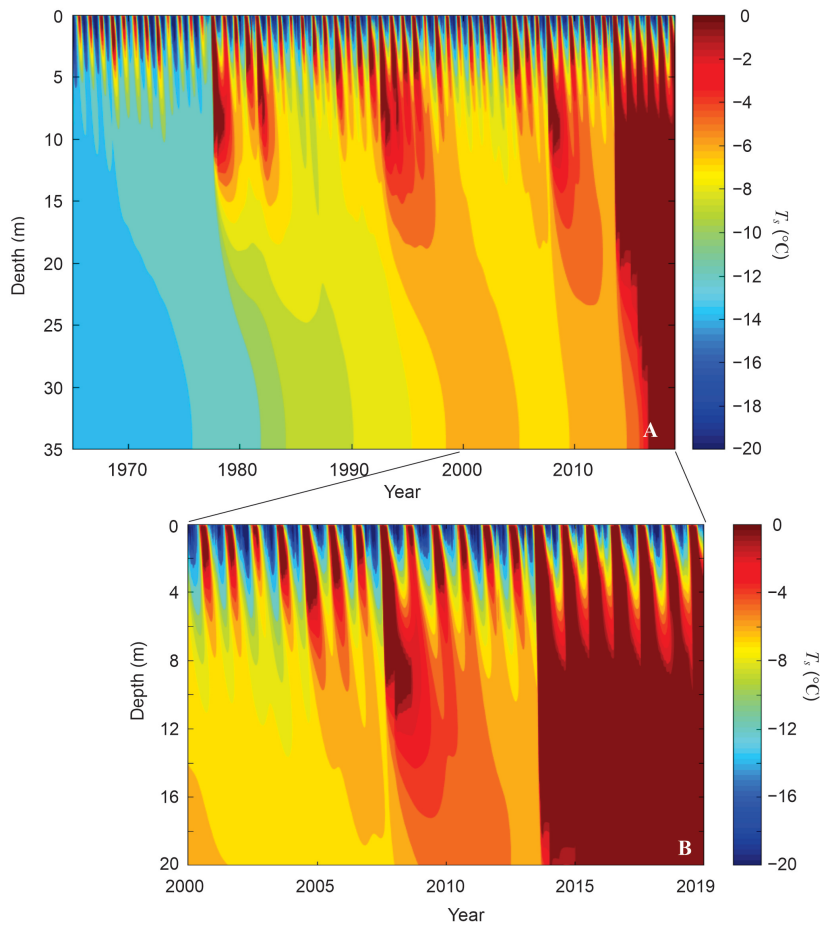
1112

l113  
l114  
l115



l116  
l117

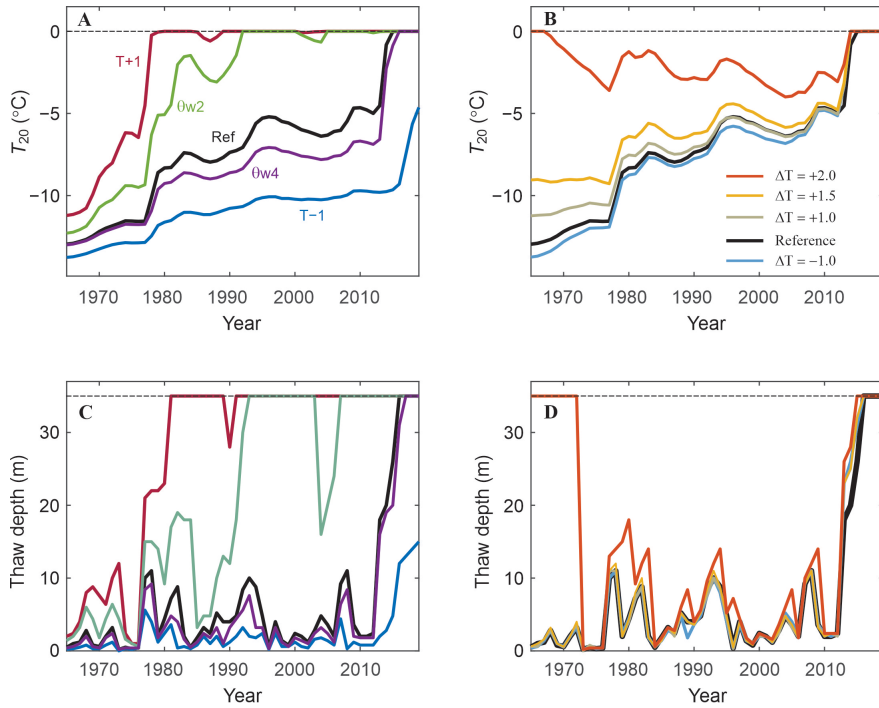
l118 **Figure 5:** Modelled meteorological, surface mass balance, and firn conditions from 1965 to 2019: (A) Summer (JJA) air and  
l119 snow-surface temperatures, °C; (B) Annual melting and 'drainage' (melting minus refreezing), mm w.e. yr<sup>-1</sup>; (C) Annual  
l120 mean snow and firn temperature at the surface (0.1 m) and at depths of 10, 20, and 35 m, °C; (D) Modelled maximum depths  
l121 of the summer wetting and thawing fronts, m; (E) Average firn density for the full firn column and in the upper 20 m, kg m<sup>-3</sup>;  
l122 (F) total firn ice content, m.  
l123



1125  
 1126  
 1127 **Figure 6:** Modelled subsurface temperature evolution for the reference model climatology and parameter settings. (A) 1965-  
 1128 2019, full 35-m firn column; (B) 2000-2019, upper 20 m. Deep temperate conditions conducive to a firn aquifer developed  
 1129 from 2013 to 2017, in response to several subsequent summers of high melting and deep meltwater infiltration.  
 1130

Luke Copland 3/8/2021 12:16 PM  
 Deleted: -

l132  
l133  
l134



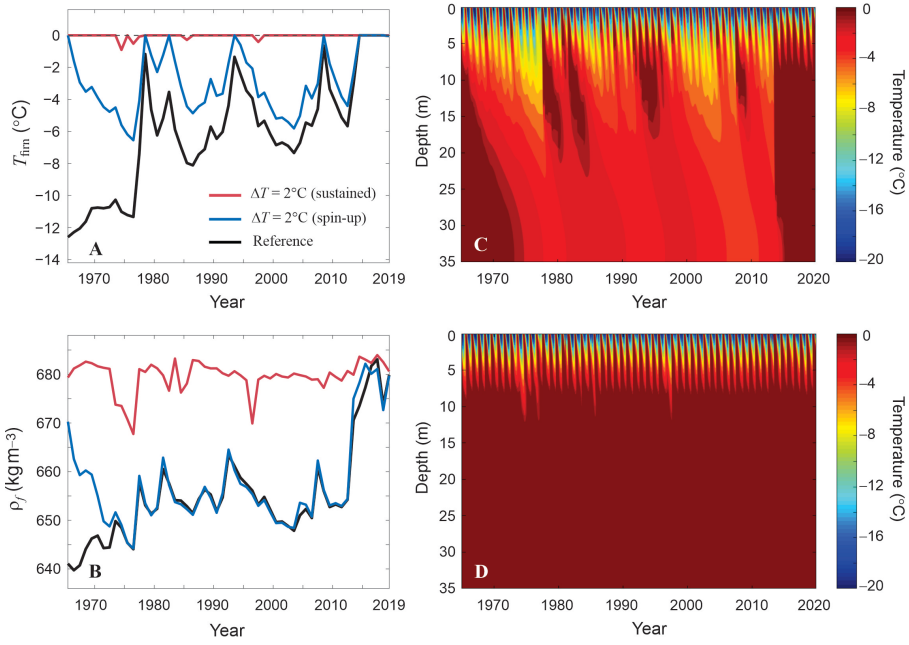
l135  
l136

l137 **Figure 7:** Sensitivity of the model simulations to (A,C) meteorological forcing and firm model parameters, and (B,D) initial  
l138 conditions, through different model spin-up settings. (A) Mean annual 20-m temperatures and (C) seasonal thaw depths from  
l139 1965-2019 for the reference model and for sensitivity experiments with  $\pm 1^\circ\text{C}$  and for irreducible water contents of 0.02  
l140 ( $\theta_{w2}$ ) and 0.04 ( $\theta_{w4}$ ). The line colours in (A) also apply to (C). An extended set of sensitivity tests is presented in the  
l141 supplementary material. (B) 20-m temperatures and (D) thaw depths from 1965-2019 after a 30-year spin-up with perpetual  
l142 1965 climatology (the reference model) and imposed temperature anomalies of 1, 1.5, 2, and  $2.5^\circ\text{C}$  for the spin-up. The  
l143 colour legend for (C) and (D) is indicated in (B).

l144  
l145  
l146

Naomi Ochwat 3/6/2021 6:55 PM  
Deleted: B





1148  
 1149  
 1150 **Figure 8:** Modelled (A) 10-m firn temperature and (B) average firn density for the reference model, for a  $2^{\circ}\text{C}$  temperature  
 1151 anomaly for the spin-up, and for a sustained temperature anomaly of  $+2^{\circ}\text{C}$ . (C,D) Firn temperature evolution for (C) the  
 1152 warm spin-up, followed by the reference climatology, and (D) sustained  $2^{\circ}\text{C}$  temperature anomalies.  
 1153